Journal of African Earth Sciences 220 (2024) 105429

Contents lists available at ScienceDirect

Journal of African Earth Sciences

journal homepage: www.elsevier.com/locate/jafrearsci

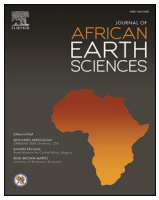

Mesozoic clastic provenance during post-rift evolution of the Essaouira Agadir Basin, Northern Morocco

Emmanuel Roquette [a], Aude Duval-Arnould [a], Orrin Bryers [a], Stefan Schröder [a,b], Tim Luber [a,c], Ian Millar [d], Rémi Charton [a,e,*], Luc Bulot [a], Jonathan Redfern [a,b]

[a] North Africa Research Group, The University of Manchester, UK
[b] Basin Studies, School of Earth and Environmental Sciences, The University of Manchester, UK
[c] Equinor, Oslo, Norway
[d] British Geological Survey, Keyworth, Nottinghamshire, UK
[e] Department of Geoscience and Engineering, Delft University of Technology, the Netherlands

ARTICLE INFO

Handling Editor: DR Damien Delvaux

Keywords:
Source-to-sink
Provenance analysis
Jurassic
Lower cretaceous
Morocco
Essaouira-agadir basin
Detrital zircon geochronology
Paleogeology modelling

ABSTRACT

This study combines several provenance tools, analysis of published structural and geodynamic data, integrated with Low-Temperature Thermochronology (LTT) and time-Temperature Modelling (tTM) to reconstruct the evolution of source-to-sink systems feeding the Essaouira-Agadir Basin (EAB) during the Jurassic (Toarcian, Bathonian, and Kimmeridgian) and Lower Cretaceous (Hauterivian and Barremian).

LTT and tTM define timing and rate of subsidence and exhumation of the hinterland and allows modelling of the predicted age and lithology of eroding rock units from the most-likely source locations through time. Extrapolation of predicted surface geology allows recognition of the lithology of sedimentary overburden in the hinterland, much of which has been subsequently eroded and is not preserved in the modern surfical geological record.

Heavy mineral, petrography and detrital zircon data analysis was carried out on fluvial and shallow marine sandstones sampled from Jurassic and Cretaceous sections across in the EAB. The results document changing sediment source terrains through time. In the Early and Middle Jurassic, the heavy mineral and detrital zircon signature correlates with a Palaeozoic source, suggesting provenance was dominantly from erosion of Cambrian and Ordovician sandstone in the Central and Western Anti-Atlas. From the Late Jurassic to Early Cretaceous, the heavy mineral and zircon signatures have a strong affinity with Triassic sediments. This indicates a provenance switch to the exhuming West Moroccan Arch (MAM and Western Meseta), interpreted to have been largely covered by Triassic continental red beds at the time.

The results help in predicting sediment delivery offshore, into the deep-water basin, where sandstones are a target for hydrocarbon exploration. Defining timing of input, location and composition helps to de-risk exploration. All the intervals examined contained discrete fluvial systems entering in the EAB, suggesting multiple periods of clastic delivery. Results suggest the Middle Jurassic and Hauterivian and Barremian intervals offer the optimum time for delivery of coarse clastics to the shelf margin, and potentially into the deep basin. The source to sink maps developed in this study further characterize these systems, their provenance and timing.

1. Introduction

Morocco, located in North-West Africa along the Central Atlantic margin, was the theatre of several oceanisation, convergence, orogenic and collision events throughout its long geological history (c.f., Michard et al., 2008a; b for a complete geological history of Morocco, used here throughout this introduction). This resulted in the creation of a complex and geologically rich country where crop out quartzite of Archean age, Quaternary sandstones and varied rocks of almost all ages in between. After the peneplanation of the Variscan orogeny which sealed the

* Corresponding author. North Africa Research Group, The University of Manchester, UK.
E-mail addresses: emmanuel.roquette@gmail.com (E. Roquette), aude.duvalarnould@gmail.com (A. Duval-Arnould), orrin.bryers@postgrad.manchester.ac.uk (O. Bryers), stefan.schroeder@manchester.ac.uk (S. Schröder), tllu@equinor.com (T. Luber), ilm@bgs.ac.uk (I. Millar), r.j.g.charton@tudelft.nl (R. Charton), jonathan.redfern@manchester.ac.uk (J. Redfern).

https://doi.org/10.1016/j.jafrearsci.2024.105429
Received 31 July 2023; Received in revised form 17 September 2024; Accepted 17 September 2024
Available online 26 September 2024

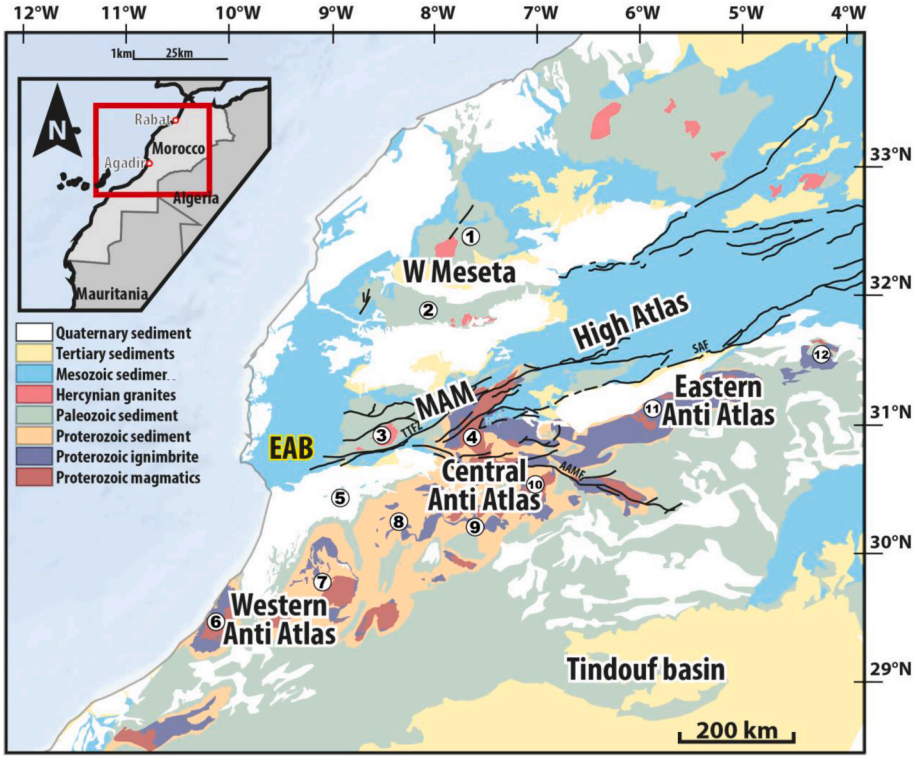

Fig. 1. Simplified geological map of the Essaouira-Agadir Basin (EAB) and hinterlands (modified from Saadi et al., 1985). 1: Rehamna, 2: Jebilets, 3: Tichka Massif, 4: Ouzellarh/Siroua region, 5: Souss Basin, 6: Ifni, 7: Kerdous, 8: Igherm, 9: Agadir-Melloul, 10: Zenaga, 11: Saghro, and 12: Ougnat (6 through 12 are the Anti-Atlas so-called inliers). 'MAM': Massif Ancien de Marrakesh, 'SAF': South Atlas Front, and 'AAMF': Anti-Atlas Major Front. The West Moroccan Arch, present during some part of the Mesozoic history of the area, was composed of present-day MAM and Western Meseta (i.e., numbers 1 through 4).

Pangaea super-continent (Variscan unconformity dated to the Late Palaeozoic), Morocco was located at the forefront of the Pangea mega-plate breakup.

Only the Atlantic N-S rift belt resulted a complete oceanisation, separating Northern Morocco from its conjugate margin: Nova Scotia. On the newly formed Atlantic shelf, the Essaouira Agadir Basin (EAB) formed at the connection between the Central Atlantic and High Atlas rifts. The EAB and its neighbouring regions recorded the extensive deposition of Triassic salt and continental facies followed by the Jurassic transgression and the establishment of open marine conditions. In the Upper Cretaceous and Cenozoic, continental scale orogenesis resulted from the African-European (Alpine) convergence and Morocco was once again thoroughly transformed. The compression created several WSW-ENE oriented mountain belts (the Anti-Atlas, High Atlas, Meseta, Middle Atlas and Rif) along with several sedimentary basins, partly reactivating and reversing normal faults created during the Mesozoic rifting (Fig. 1).

Consequently, unravelling sedimentary sources, basins, and sediment pathways at periods predating the Alpine convergence is challenging as significant differences with modern times are expected. This difficulty is increased by the recently unravelled post-rift thermal history of the margin which, far from undergoing slow thermal relaxation and subsidence, recorded abrupt and important (km-scale) denudation and burial cycles throughout the Mesozoic (e.g., Bertotti and Gouiza, 2012; Gouiza et al., 2018).

Throughout this time, there are several potential candidate hinterlands, include the Anti-Atlas, the so-called West Moroccan Arch (as defined in Frizon de Lamotte et al., 2008; i.e., parts of the High Atlas/MAM and the Western Meseta; Fig. 1). Their exhumation/subsidence histories (e.g., Gouiza et al., 2017) controlled the source, composition, grain-size, and volume of heterogeneous detritus delivered to the EAB along different pathways of sediment supply.

Most of the Late Triassic to Late Cretaceous stratigraphy in the EAB (Fig. 2) was deposited in a marine environment and from the Jurassic, relative sea level remained high. There are however five discrete regressions between the Jurassic and Lower Cretaceous, associated with progradation of fluvial systems into the basin (e.g., Charton et al., 2021b). These represent times of potential delivery of significant clastic input across the shelf and ultimately into the deep basin, and thus offer sandstone reservoir targets. They also record geodynamic changes within the hinterland. These intervals were sampled for heavy mineral analysis, detrital zircon dating and petrographic provenance analysis (Fig. 3). The dataset is complimented by a meta-analysis of geodynamic data from the surrounding hinterland, compiling time-temperature models with paleogeology modelling.

2. Geological setting

Following the collapse of the Variscan orogenic chain, Triassic to Early Jurassic extension opened three rift basins in Morocco: The Central Atlantic, Middle Atlas and High Atlas rifts (Michard et al., 2008a; b; Fig. 1). Late Triassic to Early Jurassic clastics were deposited extensively, resting unconformably on folded Palaeozoic to Precambrian basement (Piqué and Laville, 1996). A drainage divide was in the Western High Atlas cutting the Massif Ancien de Marrakech (MAM) between the Tizi N Test valley and the Oukaimeden Basin, separating the Atlantic and Tethyan domains (Beauchamp, 1988; Fabuel-Perez et al., 2009; Domènech et al., 2018; Ellouz et al., 2002). The EAB and Western MAM were located on the eastern Central Atlantic margin, and a sink for post-rift detrital sediments during the Mesozoic. The Middle and High Atlas are associated with the Tethyan domain (Frizon de Lamotte et al., 2008) and remained active rift basins until the Middle Jurassic (Ambroggi, 1963; Ellouz et al., 2002), and were inverted in the Cenozoic (e.g., Piqué et al., 2007; Leprêtre et al., 2015, 2018).

In the EAB, Permian to Triassic syn-rift continental red beds and evaporites of the Argana Formation (Beauchamp, 1988; Mader and

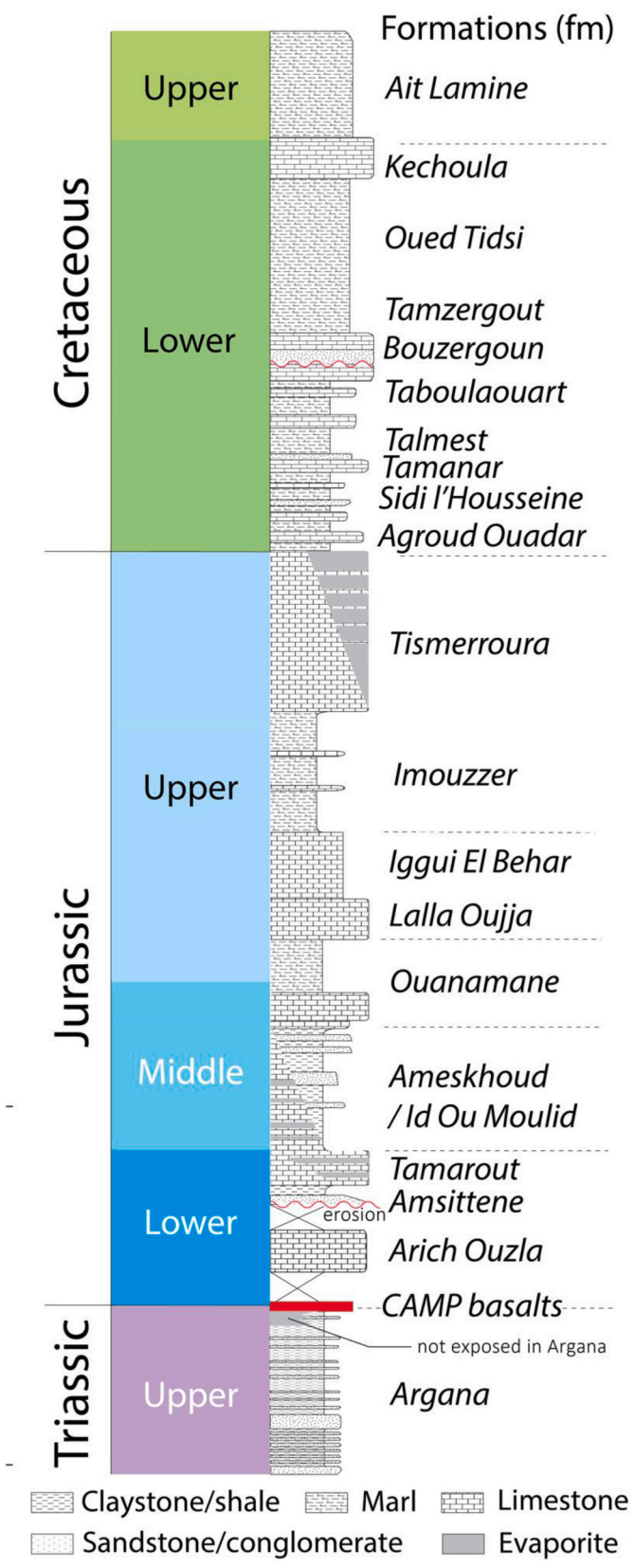

Fig. 2. Stratigraphy with Formation names of the EAB (from Charton et al., 2021b and references therein).

Redfern, 2011; 2017) have been encountered at depth by exploration wells, and form outcrops along the basin edge. These were capped by the Central Atlantic Magmatic Province (CAMP) basalts and followed by Jurassic and Cretaceous passive margin sediments, dominantly shallow marine carbonates, marls, and mudstones, but containing discrete intervals of marine and fluvial sandstones (Adams, 1979; Frizon de Lamotte et al., 2008, Duval-Arnould et al., 2021, 2024, this special issue).

The Lower Jurassic (Arich Ouzla Formation; Fig. 2) comprises carbonate-dominated lithologies, deposited on a carbonate ramp that developed during the Sinemurian and Pliensbachian (Duval-Arnould, 2019). The overlying Toarcian Amsittène Formation comprises continental siliciclastics, consisting of red fluvial conglomerates, sandstones, silts and mudstones, the latter interpreted as lacustrine, lagoonal (Ambroggi, 1963) or flood plain deposits (Ouajhain et al., 2011). In places the base is erosive, cutting down into the underlying Arich Ouzla Formation. This unconformity shows signs of exposure and karstification (Duval-Arnould, 2019). The clastics are overlain by late Toarcian peritidal carbonates, recording deepening and return to marine conditions (Fig. 2).

Most of the Middle Jurassic Ameskhoud Formation (Aalenian-Bathonian) is dominated by siliciclastics in the southern part of the EAB, evolving from shallow marine to fluvial, while the northern part (Jbel Amsittène) records dominantly shallow marine conditions (Duval-Arnould, 2019). The Ameskhoud Formation is divided into a lower and upper member. The lower member is characterized by sandy/silty dolomites with an upward gradual increase in sandstones and siltstones beds, highlighting an increasing terrestrial influx and the transition from a marine to a high-energy continental environment. The upper member comprises red mudstones with root traces, cut by channels containing coarse sandstone. This depositional environment is interpreted to be continental fluvial, episodically subjected to tidal influence (Duval-Arnould, 2019). The Middle Jurassic stratigraphy is well exposed along the Imouzzer anticline, below the main Upper Jurassic transgressive sequence.

The Ameskhoud Formation is overlain by the Upper Jurassic (Callovian) Ouanamane Formation, which at the base contains silty dolomites and oolitic grainstones. Two distinct thick limestones units, formed of reefal buildups, develop, one toward the end of the Callovian and the other in the Oxfordian (cf. Duval-Arnould et al., 2024, this special issue). In the northern part of the basin, the Callovian is dominated by peritidal carbonates, followed by deposition of mixed shoreface sediment in the middle to upper Oxfordian.

During the Kimmeridgian (Imouzzer Formation; Fig. 2) red mudstones and marls alternate with dolomitic horizons. The north and very south of the basin record important sabkha evaporites, while the centre of the basin contains thick red marls and dolomitic carbonates, indicative of an intertidal environment (Duval-Arnould, 2019). To the northeast, in the Imi N'Tanoute region, the most proximal facies is exposed, with thick continental braided fluvial sandstones, illustrating an east-west proximal to distal trend (Duval-Arnould, 2019).

Lower Cretaceous sediments in the EAB were deposited on a gently dipping shelf, which inherited its paleo-topography from the underlying Upper Jurassic carbonate ramp (Butt, 1982; Nouidar and Chellai, 2000; Rey et al., 1986a; Luber, 2017). The Hauterivian is characterized by shallow marine carbonates and mudstones of the Tamanar Formation (Rey et al., 1988). They are overlain by the Talmest Formation, which contains fluvio-deltaic red sandstones (Rey et al., 1986b), thickening to the west, where they are exposed (Wurster and Stets, 1982; Ferry et al., 2007). Co-eval fluvial red beds are also exposed along the northern bounding faults of the High Atlas, east of Imi N'Tanoute.

The Late Barremian Bouzergoun Formation contains marginal marine-littoral sandstones, vari-coloured mudstones, dolomites and interbedded thin limestones (Rey et al. 1986). A forced regression is recorded in the latest Barremian (Luber, 2017, Jaillard et al., 2019a, 2019b; Giraud et al., 2020; Bryers et al., 2024, this special issue; see also

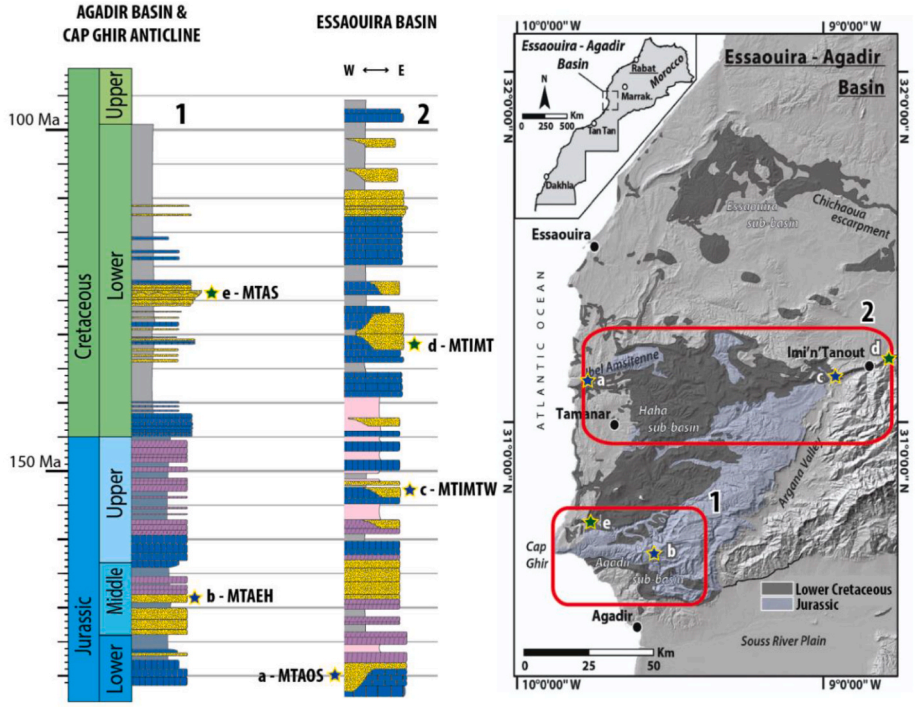

Fig. 3. Synthetic logs, in time, for the northern and southern parts of the EAB and location of the sampled fluvial systems. Section names: (a) MTAOS: Arich Ouzla Saline (b) MTAEH: Assif El (c) MTIMTW: Imi N'Tanoute West (d) MTIMT: Imi N'Tanoute, (e) MTAS: Assaka Hade.

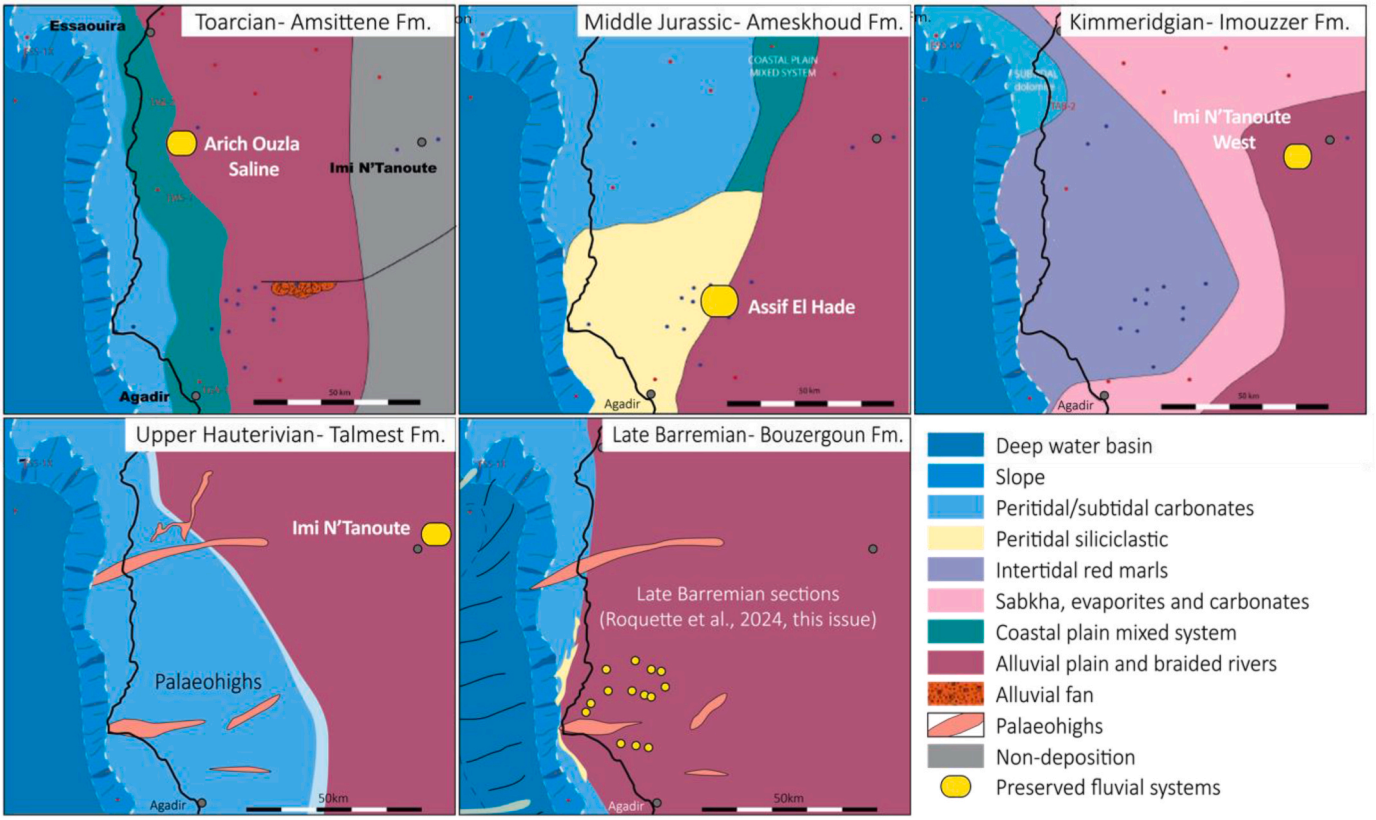

Fig. 4. Gross depositional environment maps for the Essaouira-Agadir Basin during the Jurassic and Cretaceous. Jurassic maps modified from Duval-Arnould (2019); shelf break position based on Tari et al. (2012). Cretaceous maps from Bryers et al. (2022) and published field studies (Duffaud, 1966; Rey et al., 1988; Ettachfini, 2004; Ferry et al., 2007).

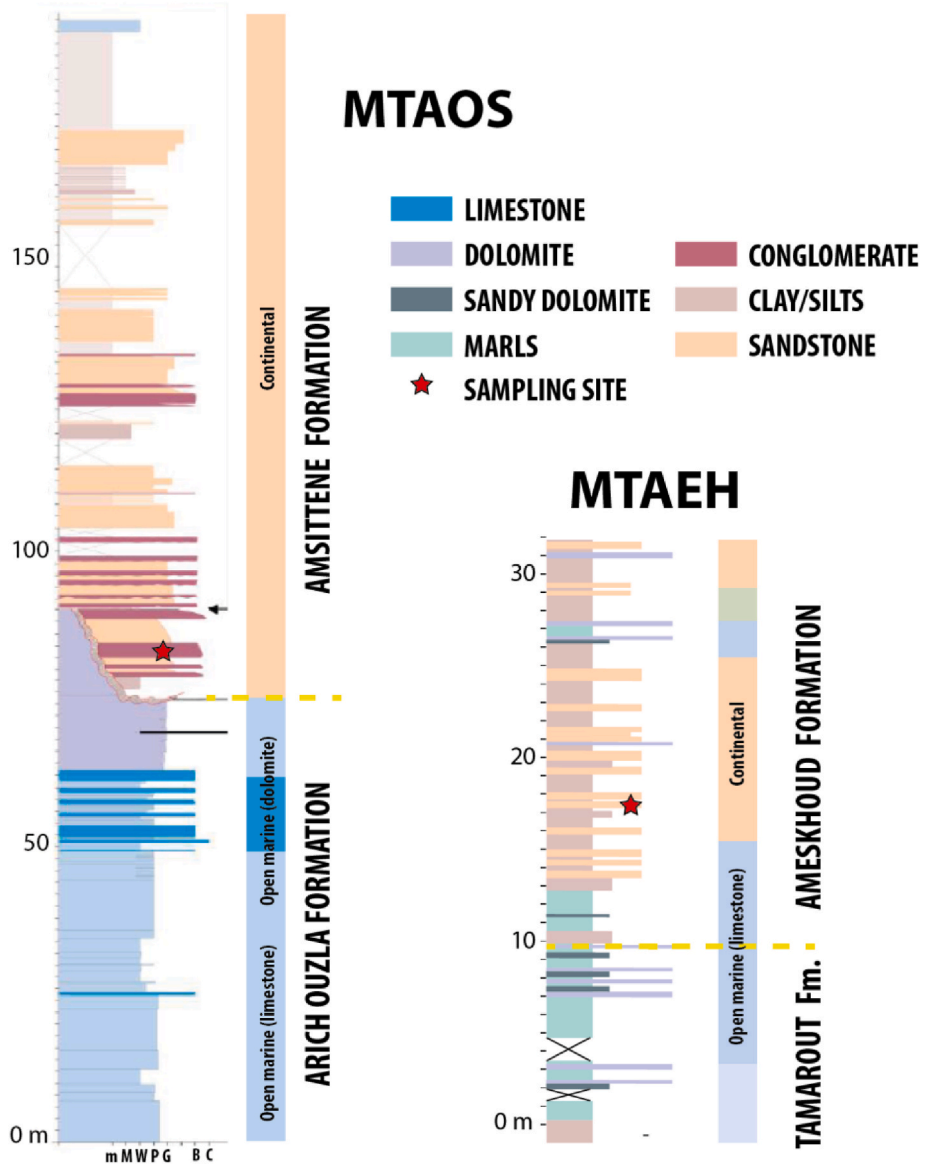

Fig. 5. Synthetic logs of Arich Ouzla Saline (MTAOS) and Assif El Hade (MTAEH) outcrops, modified from Duval-Arnould (2019). For details of lithology, sedimentary structures, fossil content, biostratigraphy, and depositional environments, see Duval-Arnould (2019) and Duval-Arnould et al. (2021).

discussion in Luber et al., in revision, this special issue), associated with an important increase in siliciclastic input and a progradation of the shoreline toward the shelf-edge (Figs. 3 and 4).

In summary, five terrestrial dominated intervals (Fig. 3), associated with regressions, are preserved as fluvial sections in the basin, in the Toarcian (Lower Jurassic), Middle Jurassic, Kimmeridgian (Upper Jurassic), Hauterivian and Barremian (Lower Cretaceous; Fig. 4). These intervals were sampled for provenance analysis.

3. Sampling locations

3.1. Arich Ouzla Saline: Toarcian (Lower Jurassic)

Toarcian fluvial systems of the Amsittène Formation are exposed in the western part of the Jbel Amsittène, northwest of the Arich Ouzla Saline (a salt mine on the western termination of the Jbel Amsittène anticline). Samples (MTAOS) were taken from the lower part of the formation, from a conglomeratic fluvial channel a few metres above an angular unconformity (see Fig. 5).

3.2. Assif El Hade Middle Jurassic

Fluvial red beds of the Middle Jurassic Ameskhoud Formation were sampled in Assif El Hade, on the northern flank of the Imouzzer anticline (Fig. 6). Samples (MTAEH): were taken from coarse sandstones approximately 8m above the top of the underlying Tamarout Formation. Samples were analysed for detrital zircon dating and heavy minerals analysis.

3.3. Imi N'Tanoute West: Kimmeridgian (Upper Jurassic)

The sampled section (MTITW) is exposed north of the Argana valley along the N8 road between Imi N'Tanoute and Argana. The section has a complete succession from the red, sand-rich Kimmeridgian down to the Oxfordian dolomitic limestones. The Kimmeridgian contains red marls with root structures and evaporitic horizons, intercalated with cross-bedded sandstones and conglomerates. Samples were taken from a section which exposed stacked channels with lateral accretion bars comprising coarse sandstones (Figs. 3–6).

In the northern part of the basin, the upper Jurassic is dominated by

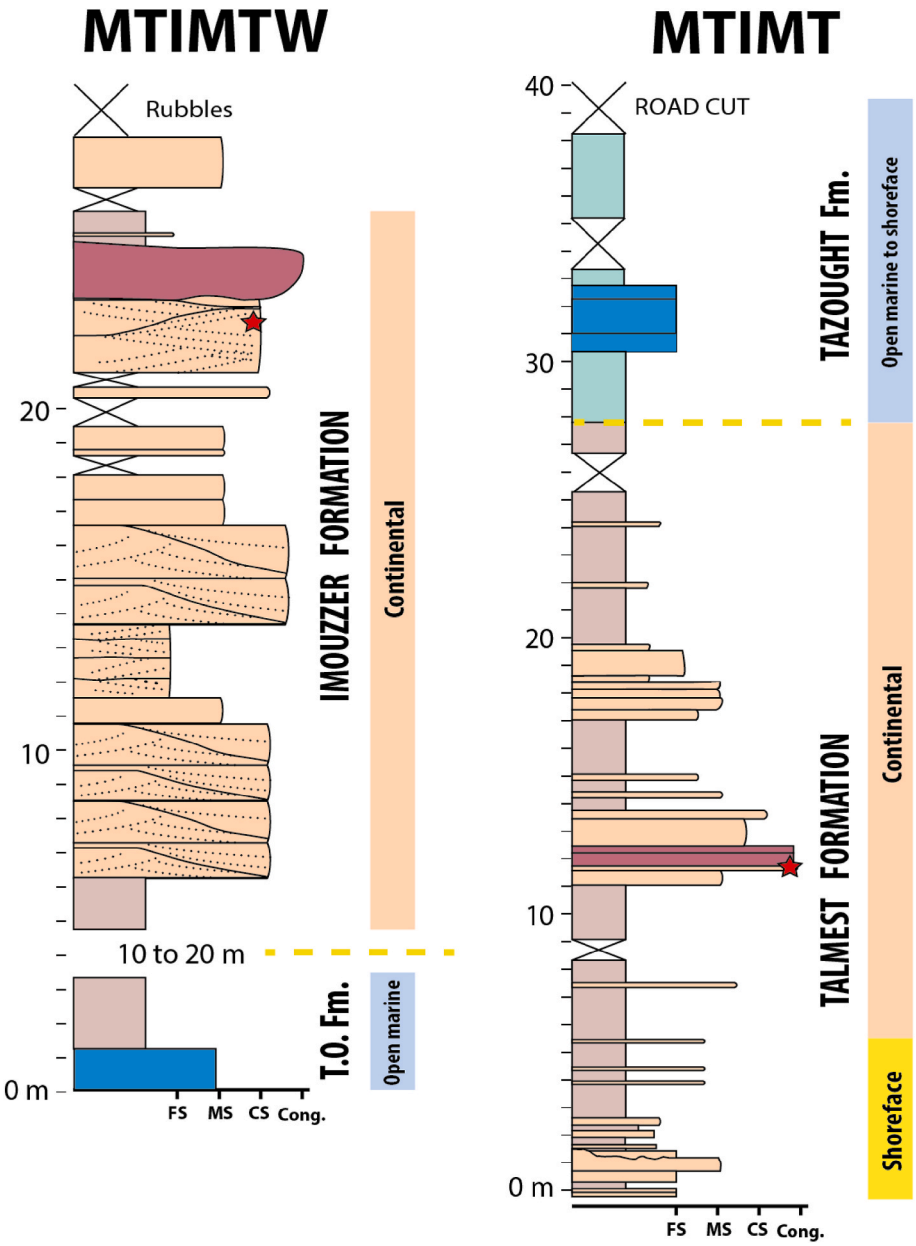

Fig. 6. Synthetic logs of the Upper Jurassic Kimmeridgian Imouzzer Fm at Imi N'Tanoute West (MTIMTW) and the Early Cretaceous Hauterivian Talmest Formation at Imi N'Tanoute (MTIMT). For details of lithology, sedimentary structures, fossil content, biostratigraphy and depositional environments, see Duval-Arnould (2019) and references therein.

peritidal carbonates until the deposition of mixed shoreface sediment in the middle to upper Oxfordian. During the Kimmeridgian, the Imouzzer Formation comprises red mudstones and marls alternating with dolomitic horizons. The north and very south of the basin record important evaporites deposited in a sabkha environment, while the centre of the basin contains thick red marls and dolomitic levels indicative of an intertidal environment (Duval-Arnould, 2019).

To the northeast, the Imi N'Tanoute region contains the most proximal equivalent of the Imouzzer Formation and records continental deposits with braided fluvial sandstones. A strong east-west proximal to distal trend is observed (Duval-Arnould, 2019).

3.4. *Imi N'Tanoute: Hauterivian (Lower Cretaceous)*

Samples (MTIMT) were taken from a roadside section exposed 1 km east of Toztane village along the P2032 road to Tabia. The section shows the transition between the Talmest and Tazought formations. Fluvial channels of the Talmest formation comprises coarse sandstones with cross stratifications, interbedded with red siltstones and mudstones. Samples were taken from the coarse sandstones from a channel a few meters below the contact with the overlying marls and limestone of the Tazought Formation (Fig. 2).

During the Hauterivian, the very low sea level allowed continental settings to prograde within the EAB. The Lower Hauterivian, characterized by the reef deposits of the Tamanar Formation, is delimited by two regional unconformities (Rey et al., 1988) and overlain by the shallower Talmest Formation. The Talmest Formation is comprised of westward thickening meandering to fluvio-deltaic red sandstones (Rey et al., 1986b) and is discussed by Ferry et al. (2007) who assume that fluvial deposits to the east grade westward to coastal plain, the shallow marine environment (near Tamanar, a locality situated near the coast between Agadir and Essaouira). Exposure of red beds in the western part

Table 1
Outcrops name, code, and coordinates of Barremian samples. Names that are marked with a "*" are merged and labelled as BFS in Tables 5 and 6 of this work (BFS standing for Barremian Fluvial Sections).

Outcrop name	Outcrop code	Latitude	Longitude
Tiskatine North*	MTTN	30,84342	−9,67121
Assaka*	MTAS	30,81406	−9,77168
Aziar North*	MTAZ	30,80863	−9,61164
Aziar*	MTDAN	30,76080	−9,58976
West Barrage/Akerkaou*	MTWB	30,75538	−9,75881
Barrage*	MTBR	30,75895	−9,68653
Tinkert*	MTTK	30,73577	−9,63322
Mahmout*	MTMH	30,72021	−9,80223
Tamri*	MTTM	30,70460	−9,82758
Addar*	MTAD	30,60226	−9,71919
Aouerga*	MTAO	30,59358	−9,64122
Tamzergout*	MTTZ	30.55127	−9.55678
Imi N'Tanout	MTIMT	31.18658	−8.76268
Imi N'Tanout West	MTIMTW	31,11199	−8,95662
Arich Ouzla Saline	MTAOS	31,16529	−9,69876
Assif El Hade	MTAEH	30,72833	−9,46454

of the basin is limited (Wurster and Stets, 1982). Fluvial red beds are exposed along the northern bounding faults of the High Atlas, east of Imi N'Tanoute. New evidence suggest that the Upper Hauterivian red deposits are fluvial to the east and grade westward to marine deposits (see Bryers et al., this special issue).

3.5. Barremian

The "Barremian-Aptian" sandstone unit (e.g., Luber, 2017) has been re-dated as late Barremian and is clearly ammonite-bearing marine deposits to the west (Jaillard et al., 2019). Neritic channels with fluvial to tidal influence of Barremian age are exposed across a large area (numerous exposures over an area of approximately 1000 km^2). The sedimentary datasets, collected by Luber et al. (2017) and coded MTTN, MTAS, MTAZ, MTDAN, MTWB, MTTK, MTMH, MTTM, MTAD, MTAO, MTTZ, and MTIMT, have their position detailed in Table 1.

4. Methods

4.1. Low-Temperature Thermochronology

The record of exhumation and subsidence of the hinterland source areas can be ascertained from analysis of Low-Temperature Thermochronology data (LTT) and resulting time-Temperature Modelling (tTM). Increasing temperature in a sample thermal history, in the absence of any igneous activity, is associated with burial, and decreasing temperature with exhumation (i.e., erosion of overburden; Fig. 7).

A large amount of thermochronology analysis has been published in the potential source domains over the last 20 years (see Charton et al., 2021a for a summary). Charton (2018) highlights that all but two of the tTM studies compiled in his meta-analysis recorded erosional exhumation. The only observed exceptions were samples from the Toubkal Massif, where tectonic exhumation created significant elevation was the preferred scenario (Ghorbal, 2009), and samples from the Canaries Islands, where episodes of regional heating, likely associated with the island volcanism, reset parts of the fission track ages (Wipf et al., 2010). This view is consistent with other previous studies which highlight that 1) samples in the Anti-Atlas in the vicinity of magmatic intrusions did not have LTT ages reset (Oukassou et al., 2013) and 2) thermal subsidence following rifting does not affect the unstretched continental crust adjacent to rift zone/rifted margins (negligible thermal relaxation; Gallagher et al., 1998).

The depth-converted tTM dataset data published in Charton et al. (2021a) was used for the modelling. Datasets were averaged in each of the six studied hinterland domains to obtain a single burial/exhumation history for the: Western, Central and Eastern Anti-Atlas, MAM and Western Meseta (Jebilets and Rehamna).

Sixteen tTM models were compiled (Fig. 8; see Table 2 and references therein), the slope gradient calculated. Each point displays the exhumation or burial through time in the different terrains. Thermochronology data is subject to large margins of error due to a modelling process, which is based on a limited number of data points (Charton, 2018; Malusà and Fitzgerald, 2019). While error margins preclude definitive interpretations for individual samples, clusters of consistent data points provide confidence that the observed trends reflect a regional behaviour.

4.2. Modelling source terrain geology through time

Using depth converted temperature paths, the composition and age of surface geology through time can be modelled (for detail of methos see Roquette et al.,2024; this special issue)). LTT datasets often record periods of subsidence (sedimentation) followed by exhumation (erosion) during which the overburden previously deposited is removed (Figs. 7–9).

During the first part of the cycle, sediments are deposited on top of

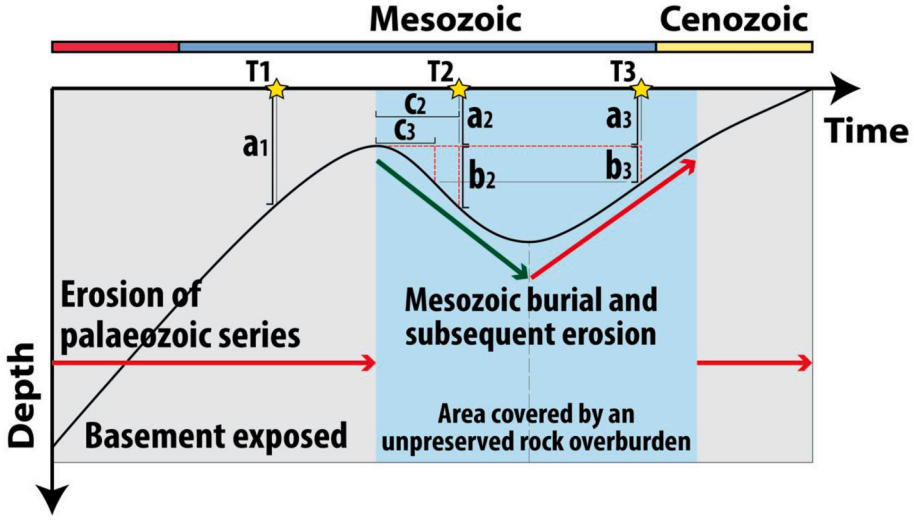

Fig. 7. Methodology to estimate the top part of the basement that was eroded away and the depth of basement/thickness of Mesozoic overburden. At times T1, T2 and T3, a is the thickness of basement, b: is the thickness of overburden and c is the age of the overburden sediments.

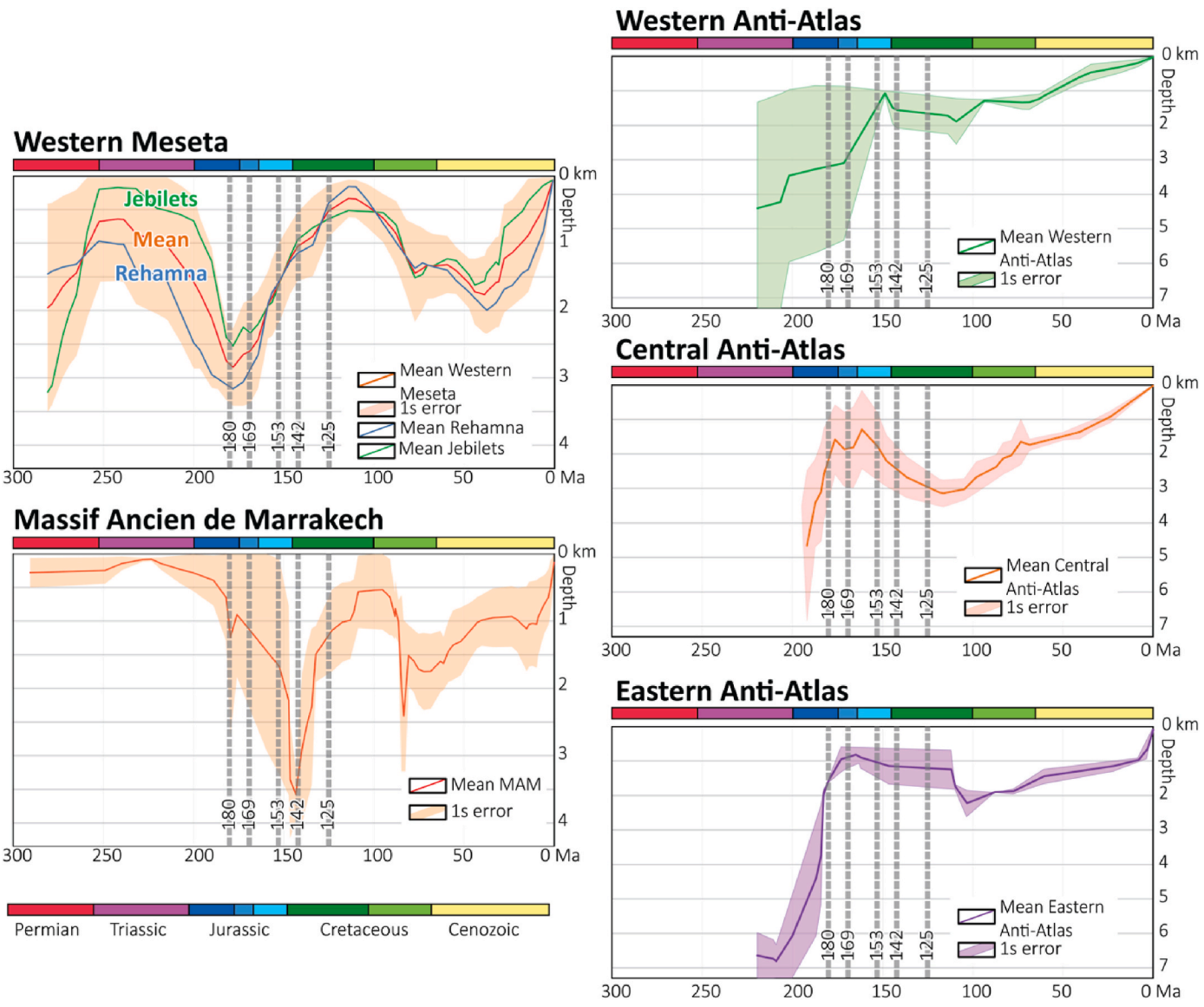

Fig. 8. Mean time-depth plots converted from tTM for the main candidate source terrains, with ages of key inflection points shown (data extracted from Charton et al., 2021a). Depth converted thermochronology data is averaged with 1 sigma error. Grey dashed line = time intervals of interest.

Table 2
Reference of LTT datasets used to constrain burial and exhumation patterns on Fig. 6.

Region	time-Temperature Models from LTT studies
Western Anti-Atlas	(Charton et al., 2018; Gouiza et al., 2017; Leprêtre, 2015; Ruiz et al., 2011; Sebti, 2011; Sehrt, 2014)
Central Anti-Atlas	(Balestrieri et al., 2009; Ghorbal, 2009; Gouiza et al., 2017; Oukassou et al., 2013)
Eastern Anti-Atlas	(Barbero et al., 2007; Gouiza et al., 2017; Malusà et al., 2007)
MAM/High Atlas	(Balestrieri et al., 2009; Barbero et al., 2007, 2011; Domènech, 2015; Ghorbal, 2009)
Western Meseta	(Ghorbal, 2009; Ghorbal et al., 2008; Sabil, 1995; Saddiqi et al., 2009; Sebti et al., 2009)

older rocks. When the region experiences exhumation, and denudation resumes, those sediments are gradually eroded. Once the overburden is completely eroded, erosion of the older strata resumes. Often, in cycles of subsidence and exhumation, the "ephemeral" overburden is totally eroded or found in isolated remnants, not preserved in the source area, and thus could not be predicted by observing the present-day geological record. It can only be identified and reconstructed using the thermal history to estimate the timing and thickness of deposition. Constraining this "ephemeral overburden" is critical, as a source region could, during such a cycle, be entirely or partly covered by lithologies mostly or entirely absent from the modern-day rock record.

4.3. Heavy mineral analysis

Samples were crushed using a jaw crusher. To minimize the number of broken grains, jaws were brought closer stepwise starting at a spacing of 2 cm. Between each step, the product was sieved at 1 mm and only the coarser fraction was re-crushed.

Samples were dry sieved at 250 μm and wet sieved at 30 μm. Six grams of crushed and sieved (30–250 μm) samples were agitated in 25 ml test tubes with 20 ml of lithium heteropolytungstate (LST, density 2.86 g/cm3). Samples were left for decantation for 3 h after which the bottom centimetre of each tube was frozen using liquid nitrogen. The bottom centimetre (heavy fraction) was recovered, mounted on glass slides, and imaged using QEMSCAN. Identified grains were then individually counted manually from the QEMSCAN maps.

On each QEMSCAN mount, all heavy minerals were individually

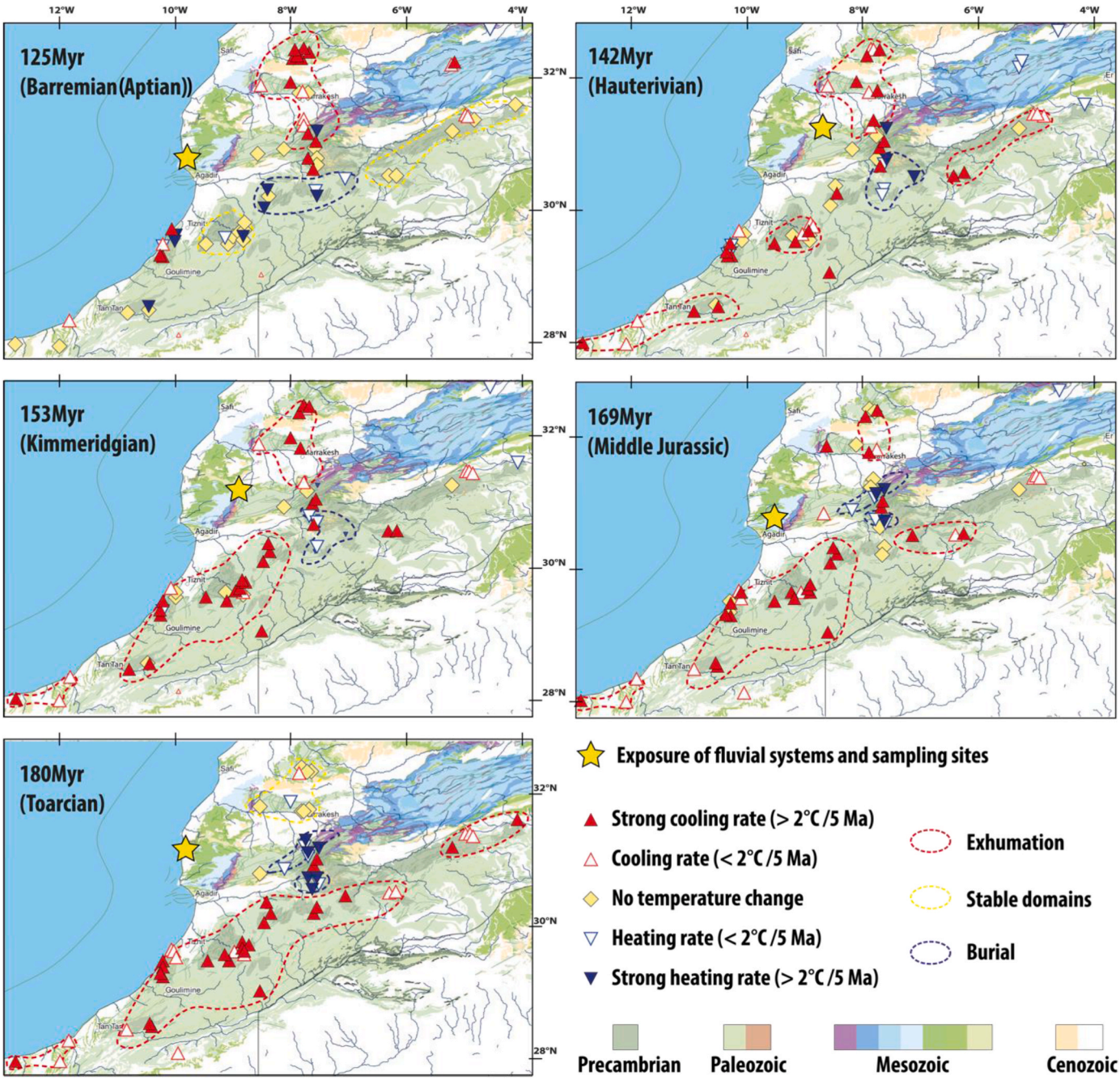

Fig. 9. Temperature evolution based on published time-temperature models for the studied periods (Charton et al., 2021a). Location of sampled coeval fluvial systems denoed by yellow star. See Table 2 for references.

counted, and percentages given thereafter are calculated based on mineral counts.

The QEMSCAN is unable to identify polymorphs of grains. Therefore, anatase and rutile could not be differentiated, and both are presented together as titanium oxides. Heavy mineral data was acquired for Toarcian, Middle Jurassic, Kimmeridgian, and Barremian samples. The small sample size did not allow for analysis of the Hauterivian sample.

4.4. Laser ablation U-Pb analysis of zircon

Five outcrops throughout the basin were selected for detrital zircon U-Pb analysis (Roquette et al.,2024). For each, samples were crushed and sieved at 30–500 μm. Heavy minerals were concentrated using a shaking table and magnetic minerals were removed using a Frantz magnetic separator. Zircons were concentrated using diiodomethane (3.3 g/cm3) and concentrates were hand-picked, mounted in epoxy disks, polished, and imaged using cathodoluminescence to select laser spots. The separation, mounting and analysis of the zircon grains was conducted at the British Geological Survey (NERC Isotope Geosciences Laboratories, Keyworth).

U-Pb analyses were carried out using a multi-collector Nu Plasma HR mass spectrometer with a New Wave 193SS solid state laser, typically using a 20–25 μm laser spot, and fluence of c. 2 J/cm^2. Laser spots were selected on core and rim of grains (though the latter were rarer) depending on the pristineness of the grain. Three standards (Plešovice zircon (Sláma et al., 2008), 91500 (Wiedenbeck et al., 1995), and GJ-1 (^{206}Pb/^{238}U 602.3 ± 1Ma, ^{207}Pb/^{206}Pb 609.2 ± 0.7Ma; in-house ID-TIMS) were regularly analysed to correct the instrument mass bias

Table 3
Model input parameters. Values were extracted from Fig. 8 using methodology presented in Roquette et al.,2024, this special issue). a = thickness of basement to reconstruct, b = thickness of sediment in the ephemeral overburden and c = age of those sediments. *Pink = basement exposed, light green = expected overburden moderate confidence, dark green = expected overburden high confidence).

Jebilets	a: thickness of removed basement to reconstruct	b: thickness of sediment in the ephemeral overburden	*	c: age of the sediments within the eph. overburden
125 Ma	150	450		Mid. Triassic
142 Ma	150	800		Mid. Tr-Low. Jur.
153 Ma	150	1450		Mid. Tr-Low. Jur.
169 Ma	150	2100		Mid. Tr-Low. Jur.
180 Ma	150	2300		Mid. Tr-Low. Jur.
Rehamna				
125 Ma	950	0		
142 Ma	950	100		Upst. Per-Mid. Tr
153 Ma	950	650		Upst. Per-Up. Tr
169 Ma	950	1650		Upst. Per-Low. Jur.
180 Ma	950	1850		Upst. Per-Low. Jur.
MAM				
125 Ma	80	1130		Up. Tr-Mid. Jur.
142 Ma	80	3200		Up. Tr-Up. Jur.
153 Ma	80	1580		Up. Tr-Up. Jur.
169 Ma	80	1050		Up. Tr-Mid. Jur.
180 Ma	80	1000		Up. Tr-Low. Jur.
Western Anti-Atlas				
125 Ma	1100	1050		Up. Jur.-Low. Cret.
142 Ma	1100	950		Up. Jur.-Low. Cret.
153 Ma	1450	0		
169 Ma	2900	0		
180 Ma	3200	0		
Central Anti-Atlas				
125 Ma	1300	1650		Up. Jur.-Low. Cret.
142 Ma	1300	1150		Up. Jur.-Low. Cret.
153 Ma	1300	550		Up. Jur.
169 Ma	1600	0		
180 Ma	2200	0		
Eastern Anti-Atlas				
125 Ma	820	400		Up. Jur.-Low. Cret.
142 Ma	820	350		Up. Jur.-Low. Cret.
153 Ma	820	230		Up. Jur.
169 Ma	900	0		
180 Ma	1600	0		

and depth dependent inter-element fractionation of U and Pb. The 91500 standard was used as primary throughout, yielding a weighted average $^{206}Pb/^{238}U$ age of 1063.9 ± 2.13 Ma (n = 108). Secondary standards Plešovice and GJ-1 gave weighted average $^{206}Pb/^{238}U$ ages of 338.3 ± 1.0 Ma (n = 79) and 602.9 ± 1.9 Ma (n = 107) respectively. Data was reduced using Iolite (Paton et al., 2010, 2011) and plotted using IsoplotR (Vermeesch, 2018).

For grains >1200 Ma in age, $^{207}Pb/^{206}Pb$ ages were used, with a discordance limit of ±10%. For grains <1200 Ma, $^{206}Pb/^{238}U$ ages were used, with a discordance limit of ±5%. Data tables and interpretations are supplied as supplementary data and are available at following url: https://bit.ly/2Zq6nBW.

Detrital zircons were recovered from Toarcian, Middle Jurassic, Hauterivian and Barremian samples. In total 175 zircon grains were dated, sampled from the Lower Jurassic Toarcian (n = 57), Middle Jurassic Bathonian (n = 46) and Lower Cretaceous Hauterivian (n = 72). The limited zircon recovery did not allow for analysis of the Kimmeridgian sample.

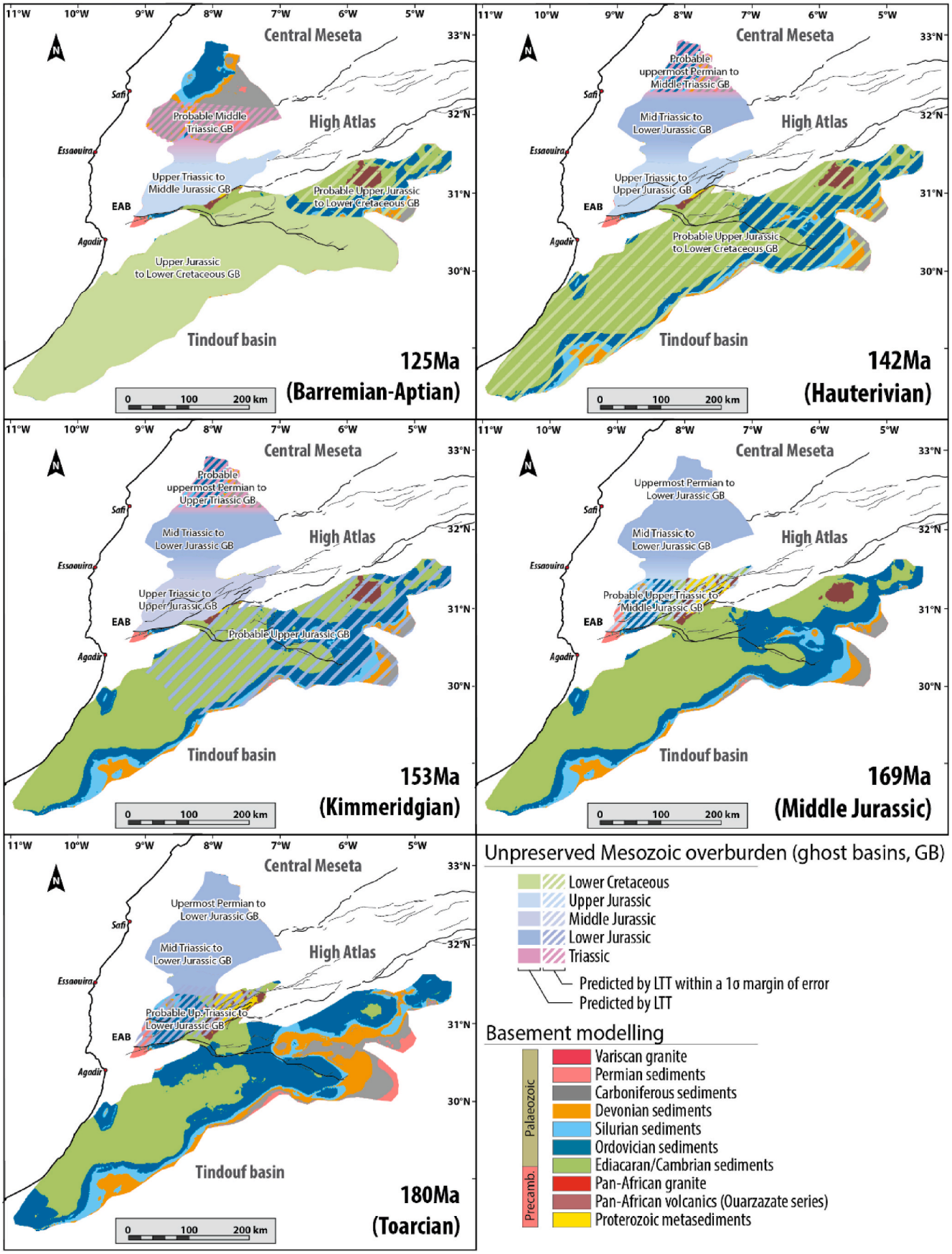

Fig. 10. Modelled age of the hinterland geology for each of the studied time intervals. Erosion values, age and thicknesses of Mesozoic sediments detailed in Table 3. GB = Ghost Basin.

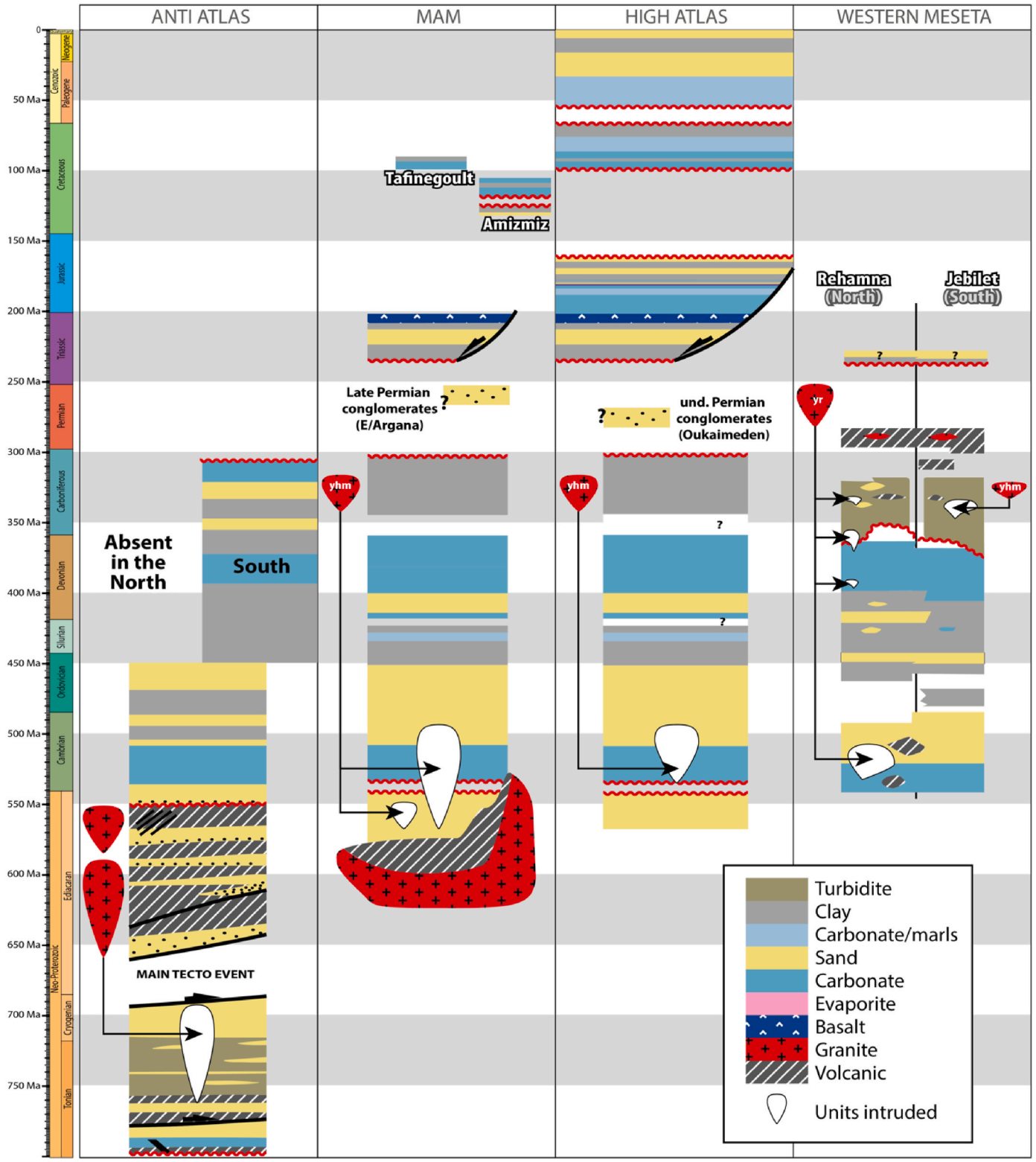

Fig. 11. Synthetic stratigraphic chart of the hinterland geology of the EAB through time: Anti-Atlas (Gasquet et al., 2005; Thomas et al., 2004), MAM and High Atlas (Beauchamp et al., 1999; Rey et al., 1986b; Saadi et al., 1985; von Rad et al., 1982; Wurster and Stets, 1982), and Western Meseta (Hoepffner et al., 2005; Piqué and Michard, 1989; Saadi et al., 1985).

5. Results

5.1. Hinterlands exhumation and burial

During the Toarcian (Fig. 9; 180Ma map) denudation occurred across the entire Anti-Atlas belt. The Western Meseta was a thermally stable domain, while the MAM was subsiding, along with parts of the Central Anti-Atlas (Siroua region).

In the Middle Jurassic (Fig. 9; 169Ma map), denudation within the Anti-Atlas decreases, while the Western Anti-Atlas continues to record

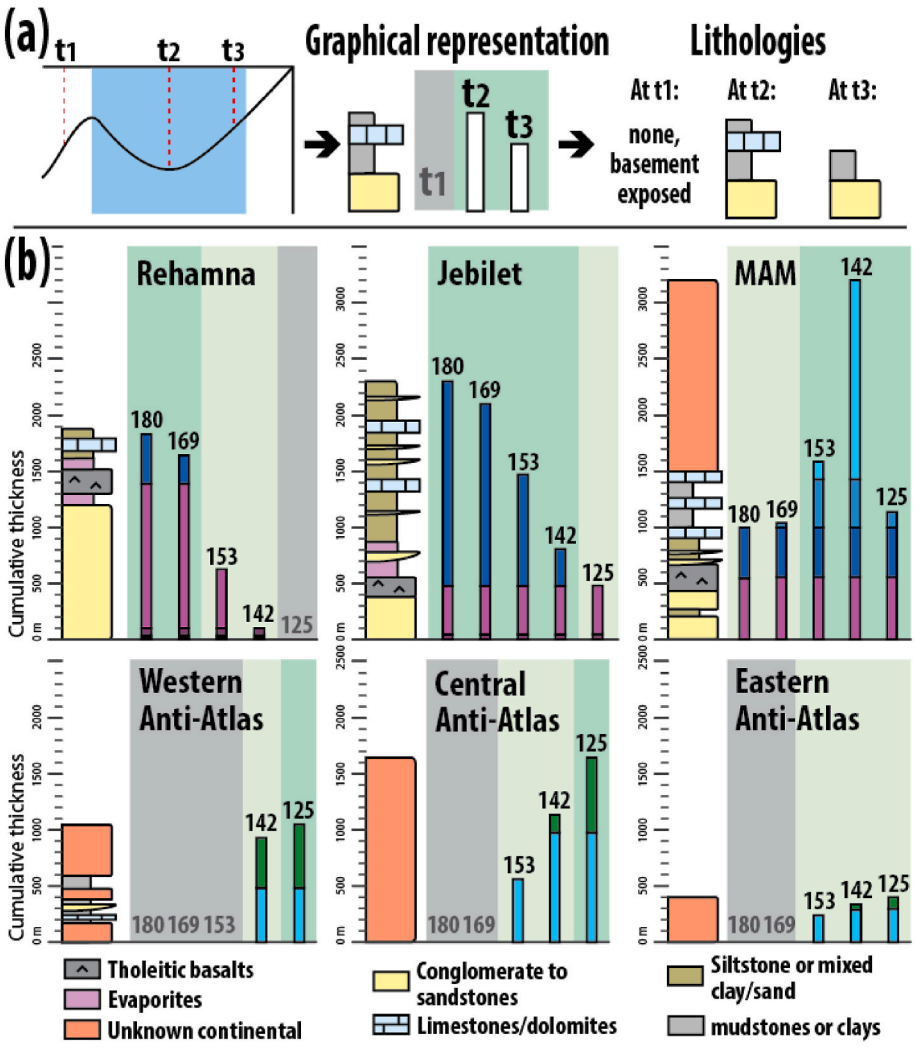

Fig. 12. Modelled overburden lithologies. (a) representation: the ages and thicknesses of unpreserved overburden taken from LTT/tTM datasets, between t1 and t2, an overburden was deposited, t2 being the maximum of thickness. Between t2 and t3, erosion removed part or all the overburden present at t2. (b) Expected lithologies within unpreserved overburdens in the EAB's hinterland at intervals of interest, see text for details and references. Dark background = basement exposed, light green = overburden predicted by tTM but within a 1σ margin of error, dark green = overburden predicted by tTM (confident).

exhumation and denudation. The Central and Eastern Anti-Atlas shows a transition to a more stable situation. In the Western Meseta, exhumation starts in the Middle Jurassic. The central MAM is still subsiding, whilst to the north and south it becomes more "stable".

In the Kimmeridgian (Fig. 9; 153Ma map), the Western Anti-Atlas consistently records exhumation, but the Central Anti-Atlas begins to subside. All 8 data points from the Western Meseta continue to record exhumation. Exhumation is recorded in the northern part of the MAM, but the behaviour of the rest of the massif remains unclear.

During the Early Cretaceous, the Western Anti-Atlas is slowly exhuming. The Hauterivian (Fig. 9; 142Ma map) data still indicates exhumation within the MAM. The Central Anti-Atlas (in Zenaga, Agadir-Melloul and south of the Siroua regions) begins to subside. The Eastern Anti-Atlas is also exhuming.

During the Late Barremian (Fig. 9; 125Ma map), the Western Meseta and MAM are the only domains recording regional exhumation. No clear evidence of exhumation is visible in the Western Anti-Atlas (data from the Kerdous inlier indicates the massif is stable). Subsidence is still recorded in the Central Anti-Atlas (Igherm, Agadir-Melloul and Zenaga regions), and the Eastern Anti-Atlas was dominantly stable.

Source terrain modelling of the age and thicknesses of possible overburden were interpreted from the LTT/tTM datasets (Fig. 9) from Charton et al., (2021a), using the methodology detailed in Roquette et al.,2024, this special issue). The obtained values used for the modelling are displayed in Table 3. A synthesis of the expected overburdens at each interval of interest is presented in Figs. 10–12.

The datasets allow reconstruction of the source terrain geology during each period for the Western Meseta (Jebilets and Rehamna massifs), the MAM, and the Western, Central and Eastern Anti-Atlas (Fig. 10).

The results show that the Proterozoic inliers, exposed today across a large part of the Anti-Atlas, were likely not exposed during the Jurassic and Lower Cretaceous. They were buried below thick Palaeozoic and Mesozoic sediments in the Jurassic, and by an additional thickness of Lower Cretaceous sediments in the Hauterivian and Barremian. The MAM and Western Meseta remained covered by Mesozoic overburden for most of the studied time interval, with Palaeozoic basement only being exposed in the Rehamna Massif in the Barremian (Figs. 10–12).

Estimation of surface lithology associated with each time unit in the geological model were based on extrapolation of know lithologies from nearby outcrops and palaeogeography/Gross Depositional Element maps (Fig. 7), with control from literature review, geological maps, and outcrop studies. A summary synthetic lithostratigraphic chart of the estimated lithologies for each source terrain is shown in Fig. 11.

LTT data indicates deposition of latest Permian overburden in the Western Meseta (Rehamna). Remnants of clastic-rich continental

Table 4
Abundance of iron oxides and dolomite in heavy mineral suites.

Sample Location	Age	Iron oxides + dolomites in heavy mineral condensate %	Number of HM grains identified (excluding FeOx and dolomite)
BFS	Barremian	62.4%	1200
MTIMTW	Kimmeridgian	71.6%	275
MTAEH	Middle Jurassic	71.2%	177
MTAOS	Toarcian	83.4%	106

Permian rocks are also preserved in the Jebilets, MAM, Argana and within narrow isolated basins (Hoepffner et al., 2005; Domeier et al., 2021; El Wartiti et al., 1990).

Lower to Upper Triassic sedimentation extended from the MAM corridor into the Argana Basin, and EAB. It was dominated by siliciclastics, sandstones and conglomerates and associated fines (mudstones and siltstones). This interpretation is based on Triassic sediments that outcrop in the Agana Basin (Mader et al., 2017), and intra montane rift basins in the Atlas/MAM (e.g. Oukaimeden basin, Tizi N Test basin) (Fabuel-Perez et al., 2009; Le Roy and Piqué, 2001), published data from exploration wells and published regional paleogeographic reconstructions (Beauchamp, 1988; Frizon de Lamotte et al., 2008; Medina, 1995). Frizon de Lamotte et al. (2008) predict the sedimentation of conglomerate and clastics across the entire Western Meseta, however, no remnants are preserved today. Triassic siliciclastics are predicted to transition laterally towards the west into finer grained units, such as the alternation of mudstones, siltstones and sandstones recorded in the DA8 well (Doukkala basin, Le Roy and Piqué, 2001). The Triassic of the EAB is capped by evaporites, though the extent of this facies to the east is uncertain (Le Roy and Piqué, 2001; Medina, 1991; Sahabi et al., 2004, Figs. 10 and 11), but according to Hafid (2000), Triassic evaporites did not extent eastward further than Imi N'Tanout.

During the Triassic-Jurassic transition, extensive tholeiitic flood basalts from the Central-Atlantic Magmatic Province (CAMP) were emplaced around the MAM region, dated to 200 ± 3 Ma (Schlische et al., 2013). The MAM was undergoing subsidence at this time (Fig. 9f) and while not preserved, CAMP basalts are expected to have been deposited widely across the region, with a calculated average thickness of 225 ± 75 m (based on 150m thick basalts in the Argana basin (west of the MAM) and 300m in the Central High Atlas (Le Roy and Piqué, 2001; Marzoli et al., 2019). Tholeiitic basalts are also documented in the

Table 5
Identification of heavy minerals grains present on QEMSCAN maps (iron oxides and dolomite fragment are ignored, see text for details.

	MTAOS - Toarcian		MTAEH - Middle Jurassic		MTIMTW - Kimmeridgian		BFS - Barr.	
	Nb. of grains	%	Nb. of grains	%	Nb. of grains	%	Nb. of grains	%
Zircon	1	0.9%	5	2.8%	11	4.0%	97	8.1%
Tourmaline	0	0.0%	13	7.3%	27	9.8%	61	5.1%
Amphiboles	8	7.5%	1	0.6%	4	1.5%	15	1.3%
Pyroxenes	4	3.8%	1	0.6%	7	2.5%	5	0.4%
Garnet	3	2.8%	5	2.8%	18	6.5%	42	3.5%
Apatite	2	1.9%	6	3.4%	50	18.2%	139	11.6%
Cr-Spinel	8	7.5%	26	14.7%	1	0.4%	4	0.3%
Olivine	1	0.9%	8	4.5%	10	3.6%	10	0.8%
TiO2	79	74.5%	112	63.3%	147	53.5%	827	68.9%
TOTAL	**106**	**100.0%**	**177**	**100.0%**	**275**	**100.0%**	**1200**	**100.0%**

Table 6
QEMSCAN data of heavy mineral mounts. For each sample, the "total vol%" column indicates the percentage of total mineral content of the mount; corrected values indicate the relative abundance of each heavy minerals after removal of dolomite, iron oxides and light minerals. (FeOx + Dol)/Heavy mineral is the ratio to the total amount of heavy minerals (including chlorite, dolomite and iron oxide).

	MTAOS - Toarcian		**MTAEH - Middle Jurassic**		**MTIMTW - Kimmeridgian**		**BFS - Barremian**	
	total vol%	Corrected Heavy mineral vol %	total vol%	Corrected Heavy mineral vol %	total vol%	Corrected Heavy mineral vol %	total vol%	Corrected Heavy mineral vol %
Zircon	0.1%	0.5%	0.1%	0.6%	0.2%	1.3%	0.9%	4.0%
Tourmaline	0.0%	0.2%	0.7%	3.9%	1.1%	5.6%	0.6%	2.8%
Amphiboles	0.5%	3.8%	0.1%	0.6%	0.7%	3.4%	0.5%	2.3%
TiO2	8.9%	73.0%	11.0%	63.0%	10.5%	53.9%	16.9%	73.3%
Pyroxenes	0.3%	2.1%	0.3%	1.8%	0.2%	1.0%	0.2%	1.1%
Garnet	0.2%	1.8%	0.6%	3.4%	1.1%	5.7%	1.1%	5.0%
Apatite	0.3%	2.1%	0.7%	4.1%	4.3%	22.3%	1.9%	8.4%
Cr-Spinel	0.7%	5.6%	1.4%	7.9%	0.0%	0.1%	0.1%	0.4%
Spinel	0.0%	0.4%	0.0%	0.2%	0.0%	0.0%	0.0%	0.1%
Sphene	0.0%	0.0%	0.0%	0.0%	0.0%	0.0%	0.0%	0.0%
Epidote	0.0%	0.0%	0.0%	0.0%	0.0%	0.0%	0.0%	0.0%
Olivine	0.5%	4.1%	1.2%	6.6%	1.3%	6.6%	0.4%	1.8%
Barite	0.8%	6.5%	1.4%	7.9%	0.0%	0.0%	0.2%	0.8%
Pyrite	0.0%	0.0%	0.0%	0.0%	0.0%	0.0%	0.0%	0.0%
Micas	0.06		0.14		0.13		0.16	
FeOx	0.32		0.41		0.31		0.23	
Dolomite	0.35		0.09		0.23		0.20	
Chlorite	0.01		0.03		0.02		0.03	
Other light minerals	0.14		0.15		0.11		0.15	
(FeOx+Dol)/Heavy min		83%		71%		72%		62%

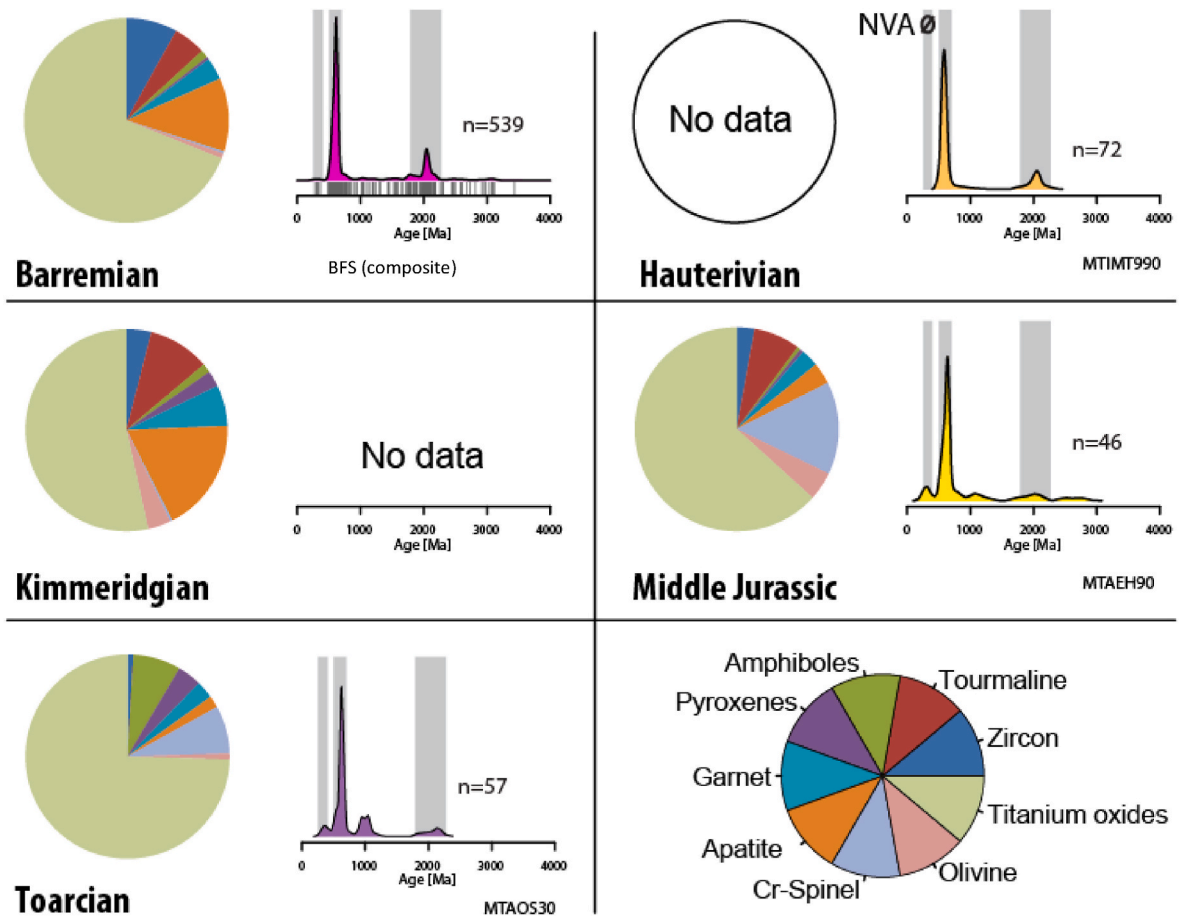

Fig. 13. Detrital zircon data (Kernel Density Plots) and heavy mineral assemblages (pie diagrams); The highlighted dominant age bands (grey bars) are Paleoproterozoic Eburnean-Birimian orogeny (2.3-1.7 Ga), Pan-African orogeny (0.8-0.54 Ga), and Variscan (0.36-0.25 Ga). Meso-Neoproterozoic around 1 Ga, Neoproterozoic peak also evident in Toarcian and Middle Jurassic samples. NVA=No Variscan Age. The compilation of detrital data for the Barremian is presented in Roquette et al.,2024) (this special issue; c.f., references therein).

Doukkala Basin (west of the Western Meseta) where they are interbedded with Hettangian-Sinemurian evaporites.

Gross depositional environment models predict a mix of carbonates, siliciclastics and mudstones deposited within continental to lagoonal/outer shelf environments (Frizon de Lamotte et al., 2008). Throughout the West Moroccan Arch, Lower to Middle Jurassic sediments are either not exposed or have been eroded.

In the Late Jurassic, the deposits across the Central Anti-Atlas and MAM are expected to be continental conglomerates, sandstones, and mudstones (Frizon de Lamotte et al., 2008; Charton et al., 2021a). The location of the Upper Jurassic palaeo-shoreline is unknown in the Western Anti-Atlas and marine incursions are possible.

5.2. Provenance analyses

5.2.1. Heavy mineral analysis

Fluvial samples were affected by dolomitization where iron oxide minerals can be found, contributing up to 83.4% of the heavy mineral suite extracted from the Toarcian sample (Tables 4–6). Nine types of heavy minerals were identified: zircon, tourmaline, amphibole, pyroxene, garnet, apatite, chrome-spinel olivine, and titanium oxides (Table 4 and Fig. 13). QEMSCAN volumetric proportions of the complete mineral content of heavy mineral mounts is provided in Table 6. The heavy mineral content is dominated in all samples by titanium oxide (53–75%), with a minor population of pyroxenes (less than 4%) and olivines (less than 5%).

The Toarcian (Lower Jurassic) fluvial sandstone sampled from the Arich Ouzla saline is dominated by titanium oxides (74.5%), chromium spinels (or Cr-spinels, 7.6%) and amphiboles (7.6%). The sample has no tourmaline and a very low yield of apatites (1.9%) and other accessory minerals (garnet 2.8%, olivine 0.9%, pyroxene 3.8% and zircons 0.9%).

In the sample Bathonian interval at Assif El Hade, Imouzzer anticline, the heavy mineral yield is also dominated by titanium oxides and Cr-spinels, but amphiboles are almost absent (0.6%). Tourmaline, absent in the Toarcian sample, accounts for 7.3% of the total in the Middle Jurassic. The sample also has important populations of apatites (3.4%), zircons (2.8%) and olivines (4.5%)

The Kimmeridgian displays an increase in the population of apatites (18.2%) and tourmalines (9.8%), and near absence of Cr-spinel (0.4%). Secondary populations of zircons (4%) and garnet (6.6%) are present.

Late Barremian samples are dominated by populations of zircon (8.1%), tourmaline (5.1%) and apatite (11.6%). Garnets account for 3.5% and amphiboles (1.3%), olivines (0.8%), pyroxene (0.4%) and Cr-spinels (0.3%) remain almost absent.

Overall, the heavy mineral record shows an increase in apatite, tourmaline and zircon, and a decrease of Cr-spinel and amphibole upwards through the Jurassic to Lower Cretaceous stratigraphy.

5.2.2. Detrital zircons

In total 175 zircon grains were sampled and dated, from the Lower Jurassic (Toarcian; n = 57), Middle Jurassic (Bathonian; n = 46) and Lower Cretaceous (Hauterivian; n = 72). The results for the Barremian are presented in this special issue (Roquette et al.,2024). All samples display the characteristic northern West African Craton (WAC) detrital

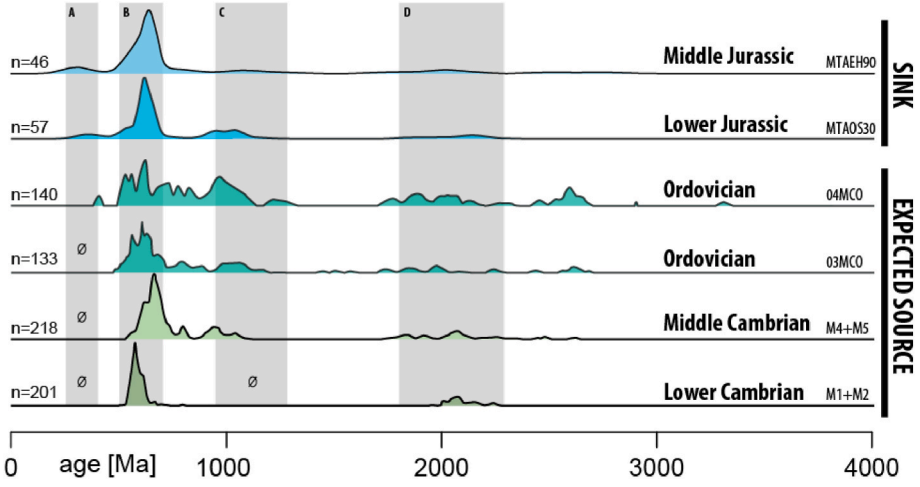

Fig. 14. Lower and Middle Jurassic detrital zircon age spectrum from samples in the EAB (analytical data from this study), showing a strong corelation with published datasets from the most-likely Palaeozoic source, the Cambrian and Ordovician from the Anti-Atlas. Cambrian data from Avigad et al. (2012), Ordovician data from Perez et al. (2019). Signatures: A = Variscan, B= Pan-African, C = Meso-Neoproterozoic, and D = Eburnean.

zircon signature. Peaks can be associated with the following orogenic events and main episodes of zircon formation: the Paleoproterozoic Eburnean-Birimian orogeny (2.3-1.7 Ga), which impacted the Reguibat Shield and formed the basement of the Anti-Atlas mobile belt (Boher et al., 1992; Gasquet et al., 2008a) and Moroccan Meseta (El Houicha et al., 2018); and the Neoproterozoic Pan-African orogeny (0.8-0.54 Ga) (Gasquet et al., 2008a; Soulaimani et al., 2018). This latter peak being dominant in all samples (Figs. 13 and 14).

In addition to the Eburnean signal, the Toarcian and Middle Jurassic samples have two secondary peaks: an important Meso-Neoproterozoic around 1.0 Ga, and a Variscan peak between 0.36 and 0.25 Ga. Jurassic samples also have a few grains indicating Paleoproterozoic to Archean ages. The Variscan population was limited in the Hauterivian sample, with rare grains associated with the Variscan Orogeny. It records the Eburnean and Pan-African populations, with rare Mesoproterozoic grains and 2 grains of ~2500 Myr age. The Barremian has a similar signature and contains the same rare zircons of Mesoproterozoic and ~2500 Myr age. No Variscan aged grains were detected.

6. Provenance of clastic sediments in the EAB

6.1. Permian and Triassic

At the end of the Variscan cycle, large amounts of sediment were eroded from the uplifted orogenic belt (estimated volume of c. 1.2×10^6 km^3 in Morocco, Charton et al., 2021a). Permian basins were a sink for deposition of continental clastics in the Western Meseta and possibly other regions (e.g., MAM, Anti-Atlas), although in the latter no Permian record remains. The extent of Permian deposits is poorly constrained, but the conglomerates and sandstone found in remnant outcrops indicate that at the time, Variscan granite bearing terranes (MAM and/or Western Meseta) were important sources of sediments (Perez et al., 2019).

In the Triassic, the onset of extensional tectonics, leading to the breakup of Pangea, saw the development of intra-montane basins that contain up to 1200 m of Middle/Upper Triassic clastic-rich sediments, deposited above Palaeozoic basement across the MAM and Western Meseta regions. Those sediments are the product of erosion of Permian and Palaeozoic terranes of the Anti-Atlas, which formed the southern rift shoulder of the newly formed High Atlas and Central Atlantic rifts. An unknown terrain was the source of Archean zircons, which also contributed to the sediment supply (Domènech et al., 2018). The Triassic-Jurassic transition is marked by the deposition of widespread tholeiitic flood basalts across the MAM and Western Meseta regions.

6.2. Jurassic

Lower-Middle Jurassic source terranes are recognised both south (Anti-Atlas) and east of the EAB (Central Anti Atlas - Siroua). Modelled LTT data derived exhumation/subsidence maps reveal that the High Atlas continued to subside during the Jurassic, with the Anti-Atlas, forming the rift shoulder, undergoing exhumation and erosion. The reconstructed surface geology for the Central and Western Anti-Atlas suggests that dominantly Cambrian to Ordovician terranes were being eroded. Despite the low zircon yield, samples from both the Lower and Middle Jurassic show strong affinity with known zircon populations from those formations. Both samples had grains within the 0.95 to 1.28-Ga age range (Figs. 13 and 14) that correlate with Ordovician (Perez et al., 2019) and Cambrian strata (Avigad et al., 2012). LTT data suggests the Western Meseta was stable at this time.

Jurassic samples also record 3 grains of Variscan age (Fig. 13), a source for which is not known from outcrop in the Anti-Atlas. Permian outcrops in the MAM that have been sampled have a significant Variscan peak, the result of weathering of MAM or Mesetian granites (Perez et al., 2019). The thickness and extent of Permian basins in Northwest Africa is poorly constrained, with only remnants remaining. However, they are expected to have been deposited widely across the region, as the product of post-orogenic peneplanation of the Variscan mountain belt. Charton et al. (2021a) estimates the volume a sediment eroded during the Permian at c. 1.2×10^6 km^3. Part of this volume would have been transported out of the region, possibly to the Reguibat Shield, but much was deposited in unpreserved Moroccan basins that probably covered the Central Anti-Atlas (Siroua), the margins of the MAM and Western Meseta. These were subsequently exhumed and eroded in the Jurassic (Charton et al., 2021a), allowing the recycling of Variscan aged zircons into Lower and Middle Jurassic sandstones. Given the dominance of the 0.95- to 1.28-Ga age range (Fig. 13), the dominant source terrain is interpreted to be the Ordovician and Middle Cambrian sediments exposed in the Central and Western Anti-Atlas, with overlying Permian rocks possibly from the MAM and Western Meseta adding a small contribution. This interpretation is supported by the heavy mineral assemblages.

The Lower and Middle Jurassic samples are characterized by their relatively high abundance of Cr-spinel and amphibole. The Central and Western Anti-Atlas are predicted to have had a thick Palaeozoic sedimentary cover during this time, with the CAMP dykes/basalts as candidate igneous source (i.e., linked to the preserved Zguid and Igherm CAMP dykes; CAMP in Morocco dated at around 201 Ma; e.g., Marzoli et al., 2019, Fig. 15). In both samples, Cr-spinel minerals are

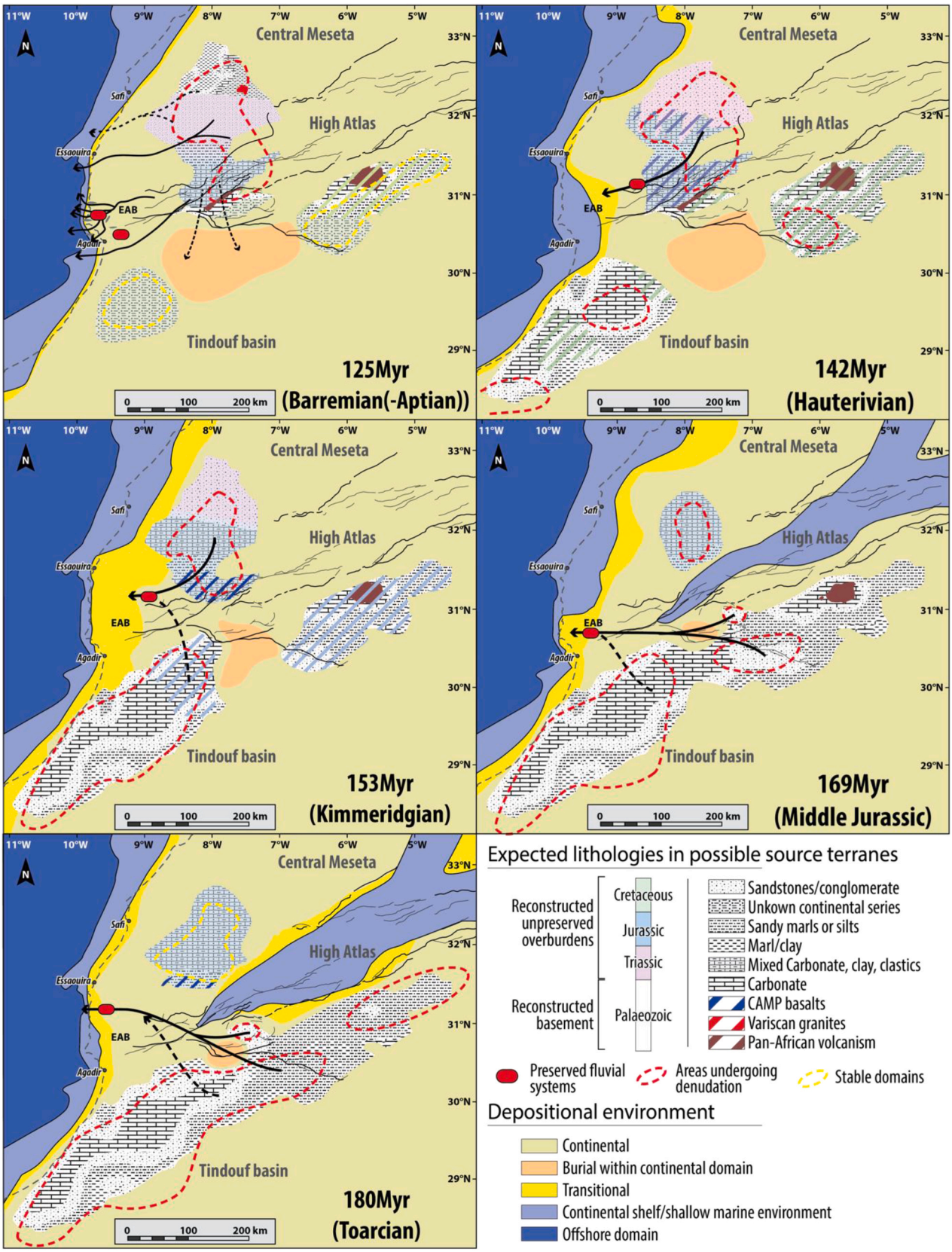

Fig. 15. Reconstructed palaeoenvironments, expected lithologies in possible source domains for each studied time interval (Toarcian, Middle Jurassic, Kimmeridgian, Hauterivian and Late Barremian (125 Ma is the transition with the Aptian)). Arrows indicate most likely provenance pathways; dashed arrows mark other possible contributions.

significantly more abundant than both olivine and pyroxenes, despite pyroxene and olivine being almost two orders of magnitude more abundant in common ultramafic rocks. Cr-spinel is a more stable mineral, that degrades less easily than olivine and pyroxenes, and as such the increased ratio is interpreted to be an indicator of weathering during transport. This is more evidence for reworking of a sediment source composed of older sandstones, ultimately derived from mafic or ultramafic rocks (Garzanti and Ando, 2019). The main candidates are the Cambrian/Ordovician sandstones found in the Bou-Azzer region of the Anti-Atlas (its S-Western-most inlier).

The combined dataset suggests the best candidate for the Toarcian and Middle Jurassic samples are Palaeozoic (Cambrian/Ordovician) and Permian sedimentary units (mudstones, sandstones, and carbonates) derived from the Central and Western Anti-Atlas (Fig. 15).

All the studied intervals contain intervals with fluvial sandstones, supporting the potential to deliver sand into the EAB, and through to the continental margin. The Toarcian and Middle Jurassic sandstones were sourced from the erosion of Ordovician and Cambrian sandstone in the Anti-Atlas. Other source lithologies, such as limestones and mudstones, were largely dissolved or disaggregated during weathering and transport and provide little contribution to the coarse clastic sediment supply.

The timing of intervals with increased sand content are interpreted to reflect sequential erosion of the hinterland. An example would be the unroofing of mudstone-rich Lower Ordovician rocks in the Anti Atlas, exposing Upper Cambrian sandstones to erosion, decreasing the sand/clay ratio during the Middle Jurassic, compared to the underling more mudstone dominated Toarcian.

In the Upper Jurassic sediments, the source location changes from the Anti-Atlas to the West Moroccan Arch. This was dominantly covered by Triassic sandstones in the Rehamna (north of the Western Meseta), sandstones, basalts and evaporites in the Jebilets (south of the Western Meseta) and sandstones, basalts, mudstones and limestones in the MAM. The Western Meseta remained a dominant regional source of sands during the Upper Jurassic with most of its products of erosion likely being shed offshore towards the west (Fig. 15).

Data suggests that the EAB was supplied largely from the erosion of the West Moroccan Arch during the Upper Jurassic, Hauterivian and Barremian. Unroofing of the Triassic, being more sand prone than the Jurassic, increased the sand/clay ratio throughout this period.

The actual routing systems of sediments to the deep-water basin during the Toarcian is unknown and sands could have been trapped on the shelf in a coastal mixed system. Reconstructions suggest that the Middle Jurassic was more clastic-rich and sediment supply may have prograded closer to the shelf margin (Charton et al., 2021b and reference therein). During that period, basin-ward tilting of the region-initiated salt movement in the offshore basin (Tari et al., 2014) and sands might have been channelised or accumulated within proximal salt-controlled mini-basins.

In the Late Jurassic, numerous salt withdrawal mini-basins are documented offshore (Tari et al., 2014; Muniz-Pichel et al., 2019). Diapir flank stratigraphic traps have been one of the main plays targeted by offshore exploration (e.g., wells RAK-1 and FA-1). However, due to the limited number of wells, control on offshore Jurassic stratigraphy remains poor. Only 3 wells within the Safi, Agadir or Tafelney basins have crossed the entire Lower Cretaceous stratigraphy and reached the Jurassic.

During the Upper Jurassic, from the Kimmeridgian onwards, modelling suggests a source shift. The relative vertical movements of the Anti-Atlas and West Moroccan Arch reverse. Exhumation in the Anti-Atlas gradually decreases, with subsidence recorded in the Central Anti-Atlas in the region of Siroua, Zenaga and north of the Agadir-Melloul inliers (Fig. 1), while exhumation and denudation is recorded in the Western Meseta and MAM. In the Western Anti-Atlas, although exhumation slows, it is still modelled to be eroding.

No detrital zircons were acquired from the Upper Jurassic sample. Results from the heavy mineral analysis show that Cr-spinels and amphiboles are almost absent, while tourmalines and apatites, which were absent from the Lower Jurassic, become prominent. The Anti-Atlas paleo-geology, at this time, is modelled to have been almost entirely covered by Palaeozoic and younger sedimentary rocks. In other words, the Anti-Atlas region in the Upper Jurassic is still locally undergoing exhumation: it is the Variscan Belt cover, made at the time of Palaeozoic and younger sediments, that is being eroded, leading to the absence of zircons in the resulting deposits in the EAB. The increase in apatite, zircon, and tourmalines at the expense of Cr-spinel and amphibole cannot be directly corelated to a specific igneous candidate source. The LTT modelling and palaeogeology reconstruction does not suggest significant unroofing to expose basement in the Anti-Atlas, and the change in heavy mineral assemblage is interpreted to indicate a change in provenance between the Anti-Atlas and the Meseta massifs (e.g., Charton et al., 2021a). Overall, the heavy mineral data is inconclusive, with no candidate source identified, but the LTT-identified exhumation (Charton et al., 2021a) and the denudation modelling suggest a change to a possible source contribution from the Western Meseta and MAM, although additional input from the Western Anti-Atlas cannot be ruled out.

6.3. Lower Cretaceous

The Hauterivian was a time of subsidence within the Central Anti-Atlas. The Western Meseta is modelled to have been largely covered by Triassic siliciclastics, and the MAM by Triassic clastics and volcanics, and Upper Jurassic sediments. No heavy mineral data was acquired from the Hauterivian section. The Hauterivian detrital zircon spectrum records exclusively Pan-African and Eburnean populations and no other diagnostic populations. Hauterivian and Barremian samples contain no zircons in the 0.95- to 1.28-Ga age range (Fig. 13) that characterize Ordovician/Cambrian strata, indicating that Palaeozoic sediments were no longer providing a significant source to the EAB.

The sampled Hauterivian intervals have a strong detrital zircon geochronology affinity with Triassic sediments, that are modelled to have covered the MAM and parts of the Western Meseta and were sourced from WAC-derived terranes with rare Variscan populations. Triassic sediments do sometimes contain an Archean zircon population, but they are not continuously recorded (Domènech et al., 2018; Marzoli et al., 2017; Perez et al., 2019).

Barremian tTM modelling shows that the Western Moroccan Arch region is exhuming at that time and is therefore a possible source candidate (Jaillard et al., 2019; Roquette et al.,2024; this special issue), but the dataset presented here does not allow discrimination between the MAM and Western Meseta (Fig. 15).

The Barremian detrital zircon age spectrum is very similar to the Hauterivian, however the large dataset (Roquette et al. 2021a) does also record a trace population of Variscan and Mesoproterozoic zircons. This corelates with the age distribution of the large sample sets published for Triassic age sandstones (Domènech et al., 2018). Heavy mineral data was analysed for the Barremian samples, and the composition supports sediment recycling, suggesting a similar source to that identified for the Kimmeridgian. Petrography of the Barremian samples (Roquette et al. 2021a) reveals rock fragment populations of limestones, sandstones and volcanics, that do not correlate with the modelled MAM overburden at the time. All the data supports a Triassic source, most probably from the Western Meseta (i.e., northern part of the West Moroccan Arch).

DSDP wells from leg 50 (Vincent et al., 1980), described with their stratigraphic logs are in or near the studied region, namely 415 (offshore Agadir), and 416 (further north and offshore Casablanca). Well 416 traversed an important section of Hauterivian clastics, more important than the Barremian one. This well is located west of the Western Mesetian massif of the Rehemna and other Variscan massifs further north. The hinterland there shows important exhumation in the Early Cretaceous, with some very strong exhumation rates for and around the Hauterivian (Charton et al., 2021a). At the well location of 415 however,

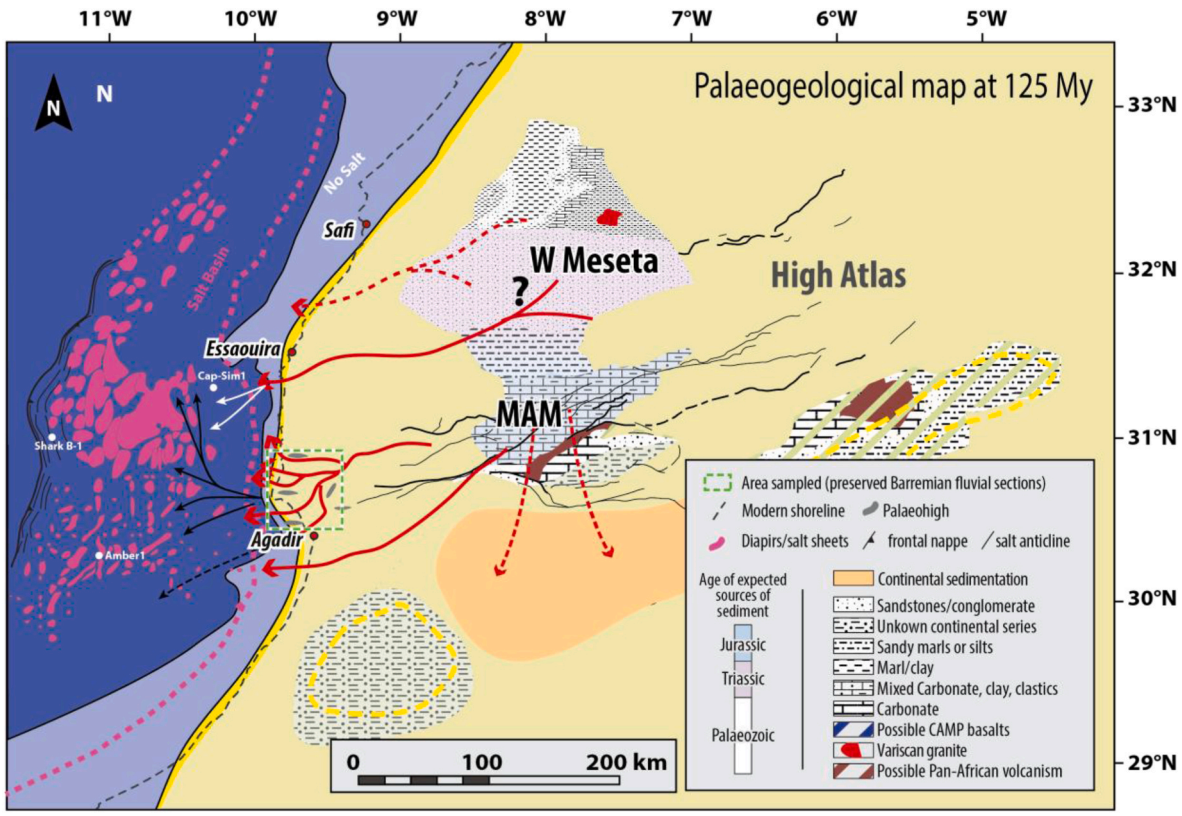

Fig. 16. Detail of Lower Cretaceous sediment source-to-sink reconstruction. See Roquette et al.,2024, this special issue) for details of onshore lithologies. MAM = Massif Ancien de Marrakech.

the well terminated in the Albian.

The latest Barremian corresponds to the strongest regression of the shoreline (Luber, 2017; Luber et al., this special issue), and is the most promising candidate for the delivery of sand to the offshore slope/basin, sourced from erosion of Triassic and older rocks that covered the MAM (Fig. 16).

7. Conclusions

A combination of several provenance tools, along with published structural and geodynamic data allowed to reconstruct the evolution of the source-to-sink systems associated with the Essaouira-Agadir Basin during the Jurassic (Toarcian, Bathonian, and Kimmeridgian) and Lower Cretaceous (Barremian).

Low-Temperature Thermochronology data highlights areas undergoing exhumation or burial. We calculate the amount of erosion and reconstruct the sedimentary sections of basins eroded. Many are ephemeral intervals that were totally eroded after deposition and are absent from the modern geology. Reconstructions based on Low-Temperature Thermochronology and predicted eroded sections were corelated with heavy mineral and detrital zircon data from samples of fluvial sandstones taken from all five intervals in the sink, the EAB. This has highlighted the reorganisation of sediment sources through time, with provenance mainly from the Central and Western Anti-Atlas during the Toarcian and Middle Jurassic, changing to the West Moroccan Arch (= MAM and Western Meseta) during the Upper Jurassic to Lower Cretaceous.

The Lower/Middle Jurassic shares a common signature with the detrital zircon population of Palaeozoic sediments from the Anti-Atlas, while the Lower Cretaceous samples have a stronger affinity with Triassic sediments of the West Moroccan Arch.

All the time intervals studied have sandstones being eroded in the hinterland and deposited in the EAB, suggesting possible clastic delivery to the offshore, however, the Middle Jurassic and Late Barremian are more clastic rich.

CRediT authorship contribution statement

Emmanuel Roquette: Writing – original draft, Visualization, Validation, Software, Resources, Methodology, Investigation, Formal analysis, Data curation, Conceptualization. **Aude Duval-Arnould:** Writing – original draft, Resources, Investigation, Formal analysis. **Orrin Bryers:** Writing – original draft, Investigation, Formal analysis. **Stefan Schröder:** Writing – review & editing, Writing – original draft, Supervision, Project administration, Methodology, Funding acquisition, Formal analysis, Data curation, Conceptualization. **Tim Luber:** Writing – review & editing, Validation, Resources, Investigation, Conceptualization. **Ian Millar:** Writing – original draft, Investigation, Data curation. **Rémi Charton:** Writing – review & editing, Writing – original draft, Visualization, Methodology, Investigation, Formal analysis, Data curation. **Luc Bulot:** Writing – original draft, Supervision, Investigation, Conceptualization. **Jonathan Redfern:** Writing – review & editing, Writing – original draft, Validation, Supervision, Resources, Project administration, Investigation, Funding acquisition, Conceptualization.

Declaration of competing interest

The authors declare that they have no known competing financial interests or personal relationships that could have appeared to influence the work reported in this paper.

Data availability

Data will be made available on request.

Acknowledgments

We wish to thank the ONHYM for the continuous support provided (data and field). We also thank the sponsors of the North Africa Research Group (NARG) for fruitful discussions. This work was undertaken as part of a NARG PhD project. We thank the anonymous reviewer and Etienne Jaillard for their very constructive feedback, enabling this work to be published. Finally, we want to express our deepest thanks to the Editor in Chief of the Journal of African Earth Sciences, Mohamed Abdel Salam.

Appendix A. Supplementary data

Supplementary data to this article can be found online at https://doi.org/10.1016/j.jafrearsci.2024.105429.

References

Adams, A.E., 1979. Sedimentary environments and palaeogeography of the western high atlas, Morocco, during the middle and late jurassic. Palaeogeogr. Palaeoclimatol. Palaeoecol. 28, 185–196. https://doi.org/10.1016/0031-0182(79)90118-4.

Ambroggi, R., 1963. Étude géologique du versant méridional du Haut Atlas occidental et de la plaine du Souss, Notes et mémoires du service géologique. Rabat.

Avigad, D., Gerdes, A., Morag, N., Bechstädt, T., 2012. Coupled U-Pb-Hf of detrital zircons of cambrian sandstones from Morocco and sardinia: implications for provenance and precambrian crustal evolution of North Africa. Gondwana Res. 21, 690–703. https://doi.org/10.1016/j.gr.2011.06.005.

Balestrieri, M.L., Moratti, G., Bigazzi, G., Algouti, A., 2009. Neogene exhumation of the Marrakech High Atlas (Morocco) recorded by apatite fission-track analysis. Terra. Nova 21, 75–82. https://doi.org/10.1111/j.1365-3121.2008.00857.x.

Barbero, L., Jabaloy, A., Gómez-Ortiz, D., Pérez-Peña, J.V., Rodríguez-Peces, M.J., Tejero, R., Estupiñán, J., Azdimousa, A., Vázquez, M., Asebriy, L., 2011. Evidence for surface uplift of the Atlas Mountains and the surrounding peripheral plateaux: combining apatite fission-track results and geomorphic indicators in the Western Moroccan Meseta (coastal Variscan Paleozoic basement). Tectonophysics 502, 90–104. https://doi.org/10.1016/j.tecto.2010.01.005.

Barbero, L., Teixell, A., Arboleya, M.L., del Rio, P., Reiners, P.W., Bougadir, B., 2007. Jurassic-to-present thermal history of the central High Atlas (Morocco) assessed by low-temperature thermochronology. Terra. Nova 19, 58–64. https://doi.org/10.1111/j.1365-3121.2006.00715.x.

Beauchamp, J., 1988. Triassic sedimentation and rifting in the high atlas. Dev. Geotectonics 22, 477–497.

Beauchamp, W., Allmendinger, R.W., Barazangi, M., Demnati, A., El Alji, M., Dahmani, M., 1999. Inversion tectonics and the evolution of the High Atlas Mountains, Morocco, based on a geological-geophysical transect. Tectonics 18, 163–184. https://doi.org/10.1029/1998TC900015.

Bertotti, G., Gouiza, M., 2012. Post-rift vertical movements and horizontal deformations in the eastern margin of the Central Atlantic: middle Jurassic to Early Cretaceous evolution of Morocco. Int. J. Earth Sci. 101, 2151–2165. https://doi.org/10.1007/s00531-012-0773-4.

Boher, M., Abouchami, W., Michard, A., Albarede, F., Arndt, N.T., 1992. Crustal growth in West Africa at 2.1 Ga. J. Geophys. Res. 97, 345–369. https://doi.org/10.1029/91JB01640.

Bryers, O., Bulot, L.G., Duval-Arnould, A., Hollis, C., Redfern, J., 2022. Kilometre-scale coral carpets on mixed carbonate-siliciclastic platforms; a sedimentological study from the Lower Cretaceous of northwestern Africa. Palaeogeogr. Palaeoclimatol. Palaeoecol. 587, 110792. https://doi.org/10.1016/j.palaeo.2021.110792.

Bryers, O., Bulot, L.G., Rehakova, D., Jeremiah, J., Ettachfini, M., Masrour, M., Casson, M., Frau, C., Pictet, A., Redfern, J., 2024. An integrated stratigraphic framework for the uppermost jurassic to Lower Cretaceous interval of the Essaouira-Agadir Basin (Moroccan Atlantic margin) based on ammonites, calcareous nannofossils and calpionellids. J. Afr. Earth Sci. https://doi.org/10.1016/j.jafrearsci.2024.105308.

Butt, A., 1982. Micropalaeontological bathymetry of the Cretaceous of western Morocco. Palaeogeogr. Palaeoclimatol. Palaeoecol. 37, 235–275.

Charton, R., 2018. Phanerozoic Vertical Movements in Morocco Phanerozoic Vertical Movements in Morocco. TU Delft, p. 174. https://doi.org/10.4233/uuid:fda35870-18d9-4ca3-9443-199a1dcb0250. PhD Thesis.

Charton, R., Bertotti, G., Arantegui, A., Bulot, L., 2018. The Sidi Ifni transect across the rifted margin of Morocco (Central Atlantic): vertical movements constrained by low-temperature thermochronology. J. Afr. Earth Sci. 141, 22–32. https://doi.org/10.1016/j.jafrearsci.2018.01.006.

Charton, R., Bertotti, G., Duval-Arnould, A., Storms, J.E.A., Redfern, J., 2021a. Low-temperature thermochronology as a control on vertical movements for semi-quantitative Source-to-Sink analysis: a case study for the Permian to Neogene of Morocco and surroundings. Basin Res. 33, 1337–1383. https://doi.org/10.1111/bre.12517.

Charton, R., Kluge, C., Fernández-Blanco, D., Duval-Arnould, A., Bryers, O., Redfern, J., Bertotti, G., 2021b. Syn-depositional Mesozoic siliciclastic pathways on the Moroccan Atlantic margin linked to evaporite mobilisation. Mar. Petrol. Geol. 128, 105018. https://doi.org/10.1016/j.marpetgeo.2021.105018.

Domeier, M., Font, E., Youbi, N., Davies, J., Nemkin, S., Van der Voo, R., Perrot, M., Benabbou, M., Boumehdi, M.A., Torsvik, T.H., 2021. On the Early Permian shape of Pangea from paleomagnetism at its core. Gondwana Res. 90, 171–198. https://doi.org/10.1016/j.gr.2020.11.005.

Domènech, M., 2015. Rift Opening and Inversion in the Marrakech High Atlas: Integrated Structural and Thermochronologic Study. PhD Thesis. Universitat Autònoma de Barcelona.

Domènech, M., Stockli, D.F., Teixell, A., 2018. Detrital zircon U–Pb provenance and palaeogeography of Triassic rift basins in the Marrakech High Atlas. Terra. Nova 30, 310–318. https://doi.org/10.1111/ter.12340.

Duval-Arnould, A.M.L.F., 2019. Controls on Stratigraphic Development of Shelf Margin Carbonates: Jurassic Atlantic Margin - Essaouira-Agadir Basin, Western Morocco. University of Manchester. PhD Thesis.

Duval-Arnould, A., Schröder, S., Charton, R., Joussiaume, R., Razin, P., Redfern, J., 2021. Early post-rift depositional systems of the central atlantic: lower and middle jurassic of the Essaouira-Agadir Basin, Morocco. J. Afr. Earth Sci. 178, 104164. https://doi.org/10.1016/j.jafrearsci.2021.104164.

Duval-Arnould, A., Bulot, L., Masrour, M., Simmons, M., Bonnot, A., Charton, R., Redfern, J., Schröder, S., 2024. A new sedimentary and biostratigraphic framework for the Callovian-Oxfordian transition on the Atlantic margin of Morocco. J. Afr. Earth Sci. 210, 105164. https://doi.org/10.1016/j.jafrearsci.2023.105164 (this special issue).

El Houicha, M., Pereira, M.F., Jouhari, A., Gama, C., Ennih, N., Fekkak, A., Ezzouhairi, H., El Attari, A., Silva, J.B., 2018. Recycling of the Proterozoic crystalline basement in the Coastal Block (Moroccan Meseta): new insights for understanding the geodynamic evolution of the northern peri-Gondwanan realm. Precambrian Res. 306, 129–154. https://doi.org/10.1016/j.precamres.2017.12.039.

El Wartiti, M., Broutin, J., Freytet, P., Larhrib, M., Toutin-Morin, N., 1990. Continental deposits in Permian basins of the Mesetian Morocco, geodynamic history. J. Afr. Earth Sci. 10, 361–368. https://doi.org/10.1016/0899-5362(90)90067-O.

Ellouz, N., Patriat, M., Gaulier, J.-M., Bouatmani, R., Sabounji, S., 2002. From rifting to Alpine inversion: Mesozoic and Cenozoic subsidence history of some Moroccan basins. Sediment. Geol. 156, 185–212. https://doi.org/10.1016/0005-2728(78)90119-6.

Fabuel-Perez, I., Hodgetts, D., Redfern, J., 2009. A new approach for outcrop characterization and geostatistical analysis of a low-sinuosity fluvial-dominated succession using digital outcrop models: upper Triassic Oukaimeden Sandstone Formation, central High Atlas, Morocco. Am. Assoc. Petrol. Geol. Bull. 93, 795–827. https://doi.org/10.1306/02230908102.

Ferry, S., Masrour, M., Grosheny, D., 2007. Le Crétacé de la marge atlantique marocaine (region d'Agadir). Excursion du Groupe Français du Crétacé. Livret-guide. https://hal.archives-ouvertes.fr/hal-00686791/fr/.

Frizon de Lamotte, D., Zizi, M., Missenard, Y., Hafid, M., El Azzouzi, M., Maury, R., Charriere, A., Taki, Z., Benammi, M., Michard, A., 2008. The atlas system. In: Continental Evolution: the Geology of Morocco: Structure, Stratigraphy, and Tectonics of the Africa-Atlantic-Mediterranean Triple Junction. Springer, Berlin, pp. 133–202.

Gallagher, K., Brown, R., Johnson, C., 1998. Fission track analysis and its applications to geological problems. Annu. Rev. Earth Planet Sci. 26, 519–572. https://doi.org/10.1146/annurev.earth.26.1.519.

Garzanti, E., Ando, S., 2019. Heavy minerals for junior woodchucks. Minerals 9, 1–25. https://doi.org/10.3390/min9030148.

Gasquet, D., Ennih, N., Liégeois, J.-P., Soulaimani, A., Michard, A., 2008. The pan-African belt. Lect. Notes Earth Sci. 116, 33–64. https://doi.org/10.1007/978-3-540-77076-3_2.

Gasquet, D., Levresse, G., Cheilletz, A., Azizi-Samir, M.R., Mouttaqi, A., 2005. Contribution to a geodynamic reconstruction of the Anti-Atlas (Morocco) during Pan-African times with the emphasis on inversion tectonics and metallogenic activity at the Precambrian-Cambrian transition. Precambrian Res. 140, 157–182. https://doi.org/10.1016/j.precamres.2005.06.009.

Ghorbal, B., 2009. Mesozoic to Quaternary Thermotectonic Evolution of Morocco (NW Africa). Vrije Universiteit Amsterdam. PhD Thesis.

Ghorbal, B., Bertotti, G., Foeken, J., Andriessen, P., 2008. Unexpected Jurassic to Neogene vertical movements in 'stable' parts of NW Africa revealed by low temperature geochronology. Terra. Nova 20, 355–363. https://doi.org/10.1111/j.1365-3121.2008.00828.x.

Giraud, F., Kassab, W.H., Robert, E., Jaillard, E., Spangenberg, J.E., Masrour, M., Hammed, M.S., Aly, M.F., El Hariri, K., 2020. Integrated stratigraphy of the latest Barremian–early Albian interval in the western part of the Tethyan margin: new data from the Essaouira-Agadir Basin (Western Morocco). Newsl. Stratigr. 54 (1), 43–78. https://doi.org/10.1127/nos/2020/0603.

Gouiza, M., Bertotti, G., Andriessen, P.A.M., 2018. Mesozoic and Cenozoic Thermal History of the Western Reguibat Shield (West African Craton). Terra Nov. https://doi.org/10.1111/ter.12318.

Gouiza, M., Charton, R., Bertotti, G., Andriessen, P., Storms, J.E.A., 2017. Post-Variscan evolution of the Anti-Atlas belt of Morocco constrained from low-temperature geochronology. Int. J. Earth Sci. 106, 593–616. https://doi.org/10.1007/s00531-016-1325-0.

Hafid, M., 2000. Triassic–early Liassic extensional systems and their Tertiary inversion, Essaouira Basin (Morocco). Mar. Petrol. Geol. 17 (3), 409–429. https://doi.org/10.1016/S0264-8172(98)00081-6.

Hoepffner, C., Soulaimani, A., Piqué, A., 2005. The Moroccan hercynides. J. Afr. Earth Sci. 43, 144–165. https://doi.org/10.1016/j.jafrearsci.2005.09.002.

Jaillard, E., Al Yacoubi, L., Reboulet, S., Robert, E., Masrour, M., Bouchaou, L., Giraud, F., El Hariri, K., 2019a. Late barremian eustacy and tectonism in the western

high atlas (Essaouira-Agadir Basin), Morocco. Cretac. Res. 93, 225–244. https://doi.org/10.1016/j.cretres.2018.08.002.
Jaillard, E., Kassab, W.H., Giraud, F., Robert, E., Masrour, M., Bouchaou, L., El Hariri, K., Hammed, M.S., Aly, M.F., 2019b. Aptian–early Albian sedimentation in the Essaouira-Agadir basin, western Morocco. Cretac. Res. 102, 59–80. https://doi.org/10.1016/j.cretres.2019.04.008.
Le Roy, P., Piqué, A., 2001. Triassic-Liassic western Moroccan synrift basins in relation to the Central Atlantic opening. Mar. Geol. 172, 359–381. https://doi.org/10.1016/S0025-3227(00)00130-4.
Leprêtre, R., 2015. Evolution phanérozoïque du Craton Ouest Africain et de ses bordures Nord et Ouest. PhD Thesis. Université Paris Sud - Paris XI.
Leprêtre, R., Missenard, Y., Barbarand, J., Gautheron, C., Jouvie, I., Saddiqi, O., 2018. Polyphased inversions of an intracontinental rift: case study of the Marrakech high atlas, Morocco. Tectonics 37, 818–841. https://doi.org/10.1002/2017TC004693.
Leprêtre, R., Missenard, Y., Saint-Bezar, B., Barbarand, J., Delpech, G., Yans, J., Dekoninck, A., Saddiqi, O., 2015. The three main steps of the Marrakech High Atlas building in Morocco: structural evidences from the southern foreland, Imini area. J. Afr. Earth Sci. 109, 177–194. https://doi.org/10.1016/j.jafrearsci.2015.05.013.
Luber, T.L., 2017. Integrated Analysis of Lower Cretaceous Stratigraphy and Depositional Systems : the Essaouira-Agadir Basin of Morocco. University of Manchester. PhD Thesis.
Luber, T.L., Bulot, L.G., Redfern, J., Frau, C., Arantegui, A., Masrour, M., 2017. A revised ammonoid biostratigraphy for the aptian of NW Africa: Essaouira-Agadir Basin, Morocco. Cretac. Res. 79, 12–34. https://doi.org/10.1016/j.cretres.2017.06.020.
Mader, N.K., Redfern, J., 2011. A sedimentological model for the continental upper triassic tadrart ouadou sandstone member: recording an interplay of climate and tectonics (Argana valley; south-west Morocco). Sedimentology 58 (5), 1247–1282. https://doi.org/10.1111/j.1365-3091.2010.01204.x.
Mader, N.K., Redfern, J., El Ouataoui, M., 2017. Sedimentology of the Essaouira Basin (Meskala Field) in context of regional sediment distribution patterns during upper Triassic pluvial events. J. Afr. Earth Sci. 130, 293–318. https://doi.org/10.1016/j.jafrearsci.2017.02.012.
Malusà, M.G., Fitzgerald, P.G., 2019. Fission-track thermochronology and its application to geology, fission-track thermochronology and its application to geology. Springer Textbooks in Earth Sciences, Geography and Environment. https://doi.org/10.1007/978-3-319-89421-8.
Malusà, M.G., Polino, R., Feroni, A.C., Ellero, A., Ottria, G., Baidder, L., Musumeci, G., 2007. Post-Variscan tectonics in eastern anti-atlas (Morocco). Terra. Nova 19, 481–489. https://doi.org/10.1111/j.1365-3121.2007.00775.x.
Marzoli, A., Bertrand, H., Youbi, N., Callegaro, S., Merle, R., Reisberg, L., Chiaradia, M., Brownlee, S.I., Jourdan, F., Zanetti, A., Davies, J.H.F.L., Cuppone, T., Mahmoudi, A., Medina, F., Renne, P.R., Bellieni, G., Crivellari, S., El Hachimi, H., Bensalah, M.K., Meyzen, C.M., Tegner, C., 2019. The central atlantic magmatic Province (CAMP) in Morocco. J. Petrol. 60, 945–996. https://doi.org/10.1093/petrology/egz021.
Marzoli, A., Davies, J.H.F.L., Youbi, N., Merle, R., Corso, J.D., Dunkley, D.J., Fioretti, A. M., Bellieni, G., Medina, F., Wotzlaw, J.-F., McHone, G., Font, E., Bensalah, M.K., 2017. Proterozoic to mesozoic evolution of North-West Africa and peri-gondwana microplates: detrital zircon ages from Morocco and Canada. Lithos 278–281, 229–239. https://doi.org/10.1016/j.lithos.2017.01.016.
Medina, F., 1991. Superimposed extensional tectonics in the Argana Triassic formations (Morocco), related to the early rifting of the Central Atlantic. Geol. Mag. 128, 525–536. https://doi.org/10.1017/S0016756800018665.
Medina, F., 1995. Syn- and postrift evolution of the El Jadida – Agadir basin (Morocco): constraints for the rifting models of the central Atlantic. Can. J. Earth Sci. 32, 1273–1291. https://doi.org/10.1139/e95-104.
Michard, A., Frizon de Lamotte, D., Saddiqi, O., Chalouan, A., 2008a. An outline of the geology of Morocco. Lect. Notes Earth Sci. 116, 1–31. https://doi.org/10.1007/978-3-540-77076-3_1.
Michard, A., Hoepffner, C., Soulaimani, A., Baidder, L., 2008b. The variscan belt. Cont. Evol. Geol. Morocco 65–132. https://doi.org/10.1007/978-3-540-77076-3_3.
Muniz Pichel, L., Huuse, M., Redfern, J., Finch, E., 2019. The influence of base-salt relief, rift topography and regional events on salt tectonics offshore Morocco. Mar. Petrol. Geol. 103, 87–113. https://doi.org/10.1016/j.marpetgeo.2019.02.007.
Nouidar, M., Chellai, E.H., 2000. Facies and sequence stratigraphy of upper barremian-lower aptian Bouzergoun Formation, Agadir Basin, Morocco. Afr. Geosci. Rev. 7, 327–340. https://doi.org/10.1006/cres.2000.0239.
Ouajhain, B., Daouidi, L., Laduron, D., Rocha, F., Naud, J., 2011. Jurassic clay mineral sedimentation control factors in the Essaouira basin (western high atlas, Morocco). Geol. Belg. 14, 129–142.
Oukassou, M., Saddiqi, O., Barbarand, J., Sebti, S., Baidder, L., Michard, A., 2013. Post-Variscan exhumation of the Central Anti-Atlas (Morocco) constrained by zircon and apatite fission-track thermochronology. Terra. Nova 25, 151–159. https://doi.org/10.1111/ter.12019.
Paton, C., Hellstrom, J., Paul, B., Woodhead, J., Hergt, J., 2011. Iolite: freeware for the visualisation and processing of mass spectrometric data. J. Anal. At. Spectrom. 26, 2508–2518. https://doi.org/10.1039/c1ja10172b.
Paton, C., Woodhead, J.D., Hellstrom, J.C., Hergt, J.M., Greig, A., Maas, R., 2010. Improved laser ablation U-Pb zircon geochronology through robust downhole fractionation correction. G-cubed 11. https://doi.org/10.1029/2009GC002618.
Perez, N.D., Teixell, A., Gómez-Gras, D., Stockli, D.F., 2019. Reconstructing extensional basin architecture and provenance in the Marrakech high atlas of Morocco: implications for rift basins and inversion tectonics. Tectonics 38, 1584–1608. https://doi.org/10.1029/2018TC005413.
Piqué, A., Laville, E., 1996. The central atlantic rifting: reactivation of paleozoic structures? J. Geodyn. 21, 235–255.
Piqué, A., Michard, A., 1989. Moroccan Hercynides: a synopsis. The paleozoic sedimentary and tectonic evolution at the northern margin of west Africa. Am. J. Sci. 289, 286–330.
Piqué, A., Soulaimani, A., Amrhar, M., Laville, E., Bouabdelli, M., Hoepffner, C., Chalouan, A., 2007. Géologie du Maroc, Géode. Marrakech.
Rey, J., Canerot, J., Peybernes, B., Taj-Eddine, K., Rahhali, K., Thieuloy, J.P., 1986a. Le Crétacé inférieur de la région d'Essaouira : données biostratigraphiques et évolutions. Rev. la Fac. des Sci. Marrakech no spécial 413–441.
Rey, J., Canérot, J., Peybernès, B., Taj-Eddine, K., Thieuloy, J.P., 1988. Lithostratigraphy, biostratigraphy and sedimentary dynamics of the Lower Cretaceous deposits on the northern side of the western High Atlas (Morocco). Cretac. Res. 9, 141–158. https://doi.org/10.1016/0195-6671(88)90014-6.
Rey, J., Canerot, J., Rocher, A., Taj-Eddine, K., Thieuloy, J.P., 1986b. Le Crétacé inférieur sur le versant nord du Haut-Atlas (région d'Imi n'Tanout et Amizmiz) données biostratigraphiques et évolutions sédimentaires. Rev. la Fac. des Sci. Marrakech 183, 393–441.
Roquette, E., Lovell-Kennedy, J., Muniz Pichel, L., Schröder, S., Charton, R., Millar, I., Frau, C., Redfern, J., 2024. Integrated multi-proxy source-to-sink analysis of late barremian (lower cretaceous) clastic systems in the Essaouira-Agadir Basin. J. Afr. Earth Sci. 2024. https://doi.org/10.1016/j.jafrearsci.2024.105205 (this special issue).
Ruiz, G.M.H., Sebti, S., Negro, F., Saddiqi, O., Frizon de Lamotte, D., Stockli, D., Foeken, J., Stuart, F., Barbarand, J., Schaer, J.P., 2011. From central Atlantic continental rift to Neogene uplift - western Anti-Atlas (Morocco). Terra. Nova 23, 35–41. https://doi.org/10.1111/j.1365-3121.2010.00980.x.
Saadi, M., Hilali, E.A., Bensaid, M., Boudda, A., Dahmani, M., 1985. Carte Géologique de Maroc. Ministère l'Énergie des Mines, Dir. la Géologie.
Sabil, N., 1995. La datation par traces de fission: aspects méthodologiques et applications thermochronologiques en contexte alpin et de marge continentale. PhD Thesis. Université Joseph Fourier - Grenoble I.
Saddiqi, O., El Haimer, F.Z., Michard, A., Barbarand, J., Ruiz, G.M.H., Mansour, E.M., Leturmy, P., Frizon de Lamotte, D., 2009. Apatite fission-track analyses on basement granites from south-western Meseta, Morocco: paleogeographic implications and interpretation of AFT age discrepancies. Tectonophysics 475, 29–37. https://doi.org/10.1016/j.tecto.2009.01.007.
Sahabi, M., Aslanian, D., Olivet, J.-L., 2004. Un nouveau point de départ pour l'histoire de l'Atlantique central. Compt. Rendus Geosci. 336, 1041–1052.
Schlische, R.W., Withjack, M.O., Olsen, P.E., 2013. Relative timing of CAMP, rifting, continental breakup, and basin inversion: tectonic significance. Geophys. Monogr. 136, 33–59. https://doi.org/10.1029/136GM03.
Sebti, S., 2011. Mouvements verticaux de l'Anti-Atlas occidental marocain (Kerdous and Ifni): Thermochronologie par traces de fission. Université Hassan II. PhD Thesis.
Sebti, S., Saddiqi, O., El Haimer, F.Z., Michard, A., Ruiz, G., Bousquet, R., Baidder, L., Frizon de Lamotte, D., 2009. Vertical movements at the fringe of the West African Craton: first zircon fission track datings from the Anti-Atlas Precambrian basement, Morocco. Compt. Rendus Geosci. 341, 71–77. https://doi.org/10.1016/j.crte.2008.11.006.
Sehrt, M., 2014. Variscan to Neogene long-term landscape evolution at the Moroccan passive continental margin (Tarfaya Basin and western anti-Atlas). PhD Thesis. Ruprecht-Karls-Universität Heidelberg.
Sláma, J., Košler, J., Condon, D.J., Crowley, J.L., Gerdes, A., Hanchar, J.M., Horstwood, M.S.A., Morris, G.A., Nasdala, L., Norberg, N., Schaltegger, U., Schoene, B., Tubrett, M.N., Whitehouse, M.J., 2008. Plešovice zircon - a new natural reference material for U-Pb and Hf isotopic microanalysis. Chem. Geol. 249, 1–35. https://doi.org/10.1016/j.chemgeo.2007.11.005.
Soulaimani, A., Ouanaimi, H., Saddiqi, O., Baidder, L., Michard, A., 2018. The anti-atlas pan-african belt (Morocco): overview and pending questions. Compt. Rendus Geosci. 350, 279–288. https://doi.org/10.1016/j.crte.2018.07.002.
Tari, G., Brown, D., Jabour, H., Hafid, M., Louden, K., Zizi, M., 2012. 8 - the conjugate margins of Morocco and Nova Scotia. In: Roberts, D.G., Bally, A.W. (Eds.), Regional Geology and Tectonics: Phanerozoic Passive Margins, Cratonic Basins and Global Tectonic Maps. Elsevier B.V., pp. 284–323. https://doi.org/10.1016/B978-0-444-56357-6.00007-X
Tari, G., Jabour, H., Tari, G., Jabour, H., 2014. Salt tectonics along the Atlantic margin of Morocco Salt tectonics along the Atlantic margin of Morocco. Conjug. Divergent Margins 337–353. https://doi.org/10.1144/SP369.23.
Thomas, R.J., Fekkak, A., Ennih, N., Errami, E., Loughlin, S.C., Gresse, P.G., Chevallier, L. P., Liégeois, J.-P., 2004. A new lithostratigraphic framework for the Anti-Atlas Orogen, Morocco. J. Afr. Earth Sci. 39, 217–226. https://doi.org/10.1016/j.jafrearsci.2004.07.046.
Vermeesch, P., 2018. IsoplotR: a free and open toolbox for geochronology. Geosci. Front. 9, 1479–1493. https://doi.org/10.1016/j.gsf.2018.04.001.
von Rad, U., Hinz, K., Sarnthein, M., Seibold, E., 1982. Geology of the Northwest African Continental Margin. Springer-V. ed. Berlin Heidelberg, New York. https://doi.org/10.1007/978-3-642-68409-8.
Wiedenbeck, M., Allé, P., Corfu, F., Griffin, W.L., Meier, M., Oberli, F., Quadt, A.V.O.N., Roddick, J.C., Spiegel, W., 1995. Three natural zircon standards for U-Th-Pb, Lu-Hf, trace element and ree analyses. Geostand. Newsl. 19, 1–23. https://doi.org/10.1111/j.1751-908X.1995.tb00147.x.
Wipf, M., Glasmacher, U.A., Stockli, D.F., Emmerich, A., Bechstädt, T., Baur, H., 2010. Reconstruction of the differentiated long-term exhumation history of Fuerteventura, Canary Islands, Spain, through fission-track and (U-Th-Sm)/He data. Int. J. Earth Sci. 99, 675–686. https://doi.org/10.1007/s00531-008-0415-z.
Wurster, P., Stets, J., 1982. Sedimentation in the atlas gulf II: mid-cretaceous events. In: von Rad, U., Hinz, K., Sarnthein, M., Seibold, E. (Eds.), Geology of the Northwest African Continental Margin. Springer Berlin Heidelberg, Berlin, pp. 439–458.